MAS2-CT94-0087 -Berm Breakwaters Structures-
Final Workshop, Reykjavik, 4 November 1996

RESHAPING BREAKWATER: DESCRIPTION OF THE PROFILE EVOLUTION

by

R. Archetti[1] , A. Lamberti[1]

Abstract

In order to develop a model able to describe how berm breakwaters reshape under the attack of waves, a large quantity of data from 2D and 3D tests was collected and arranged in a database. The data were first standardised, and since data come from models with very different size, all the lengths were scaled with the nominal diameter (D_{n50}) of berm stones. Since the information regarding the wave conditions in shallow water or in front of the breakwater was not always available the wave conditions were estimated in front of the breakwater by using formulae proposed by Goda (1985) and Stive, (1986).
The profiles were schematised as suggested by Vellinga (1986) and van der Meer (1988) using six parameters; with the aid of PCA the original variables were transformed into uncorrelated components describing decreasing quotes of the total variance. Three of them account for 95% of the variance of our data-base.
In this manner the dimensionality of the phenomenon was reduced from six to three. Each component describes part of the behaviour of the reshaping breakwater and for each of them a model was developed relating components to the environmental and structural parameters.
The model respects approximately (relatively to the 1st PC) the composition principle and gives results for any condition. At the end the model was compared with the experimental profiles and with the output of BREAKWAT©, the software developed by DH for the conceptual design of rubble mound structures.

1. INTRODUCTION

Berm or reshaping breakwaters represent a relatively new type of wave barriers; more precisely the conscious acceptance of stone movement during reshaping and of the

[1] DISTART. Università degli studi di Bologna. Viale Risorgimento,2 I 40136 Bologna.

possible dynamic equilibrium of the units in the exposed mound is new. In fact, the coasts are full of gravel beaches and deformed mounds.
It is accepted that the stones of the armour layer move under the wave attack until a new equilibrium of the seaward profile is formed.

Van der Meer (1988) studied the shape of the profile, and developed a model representing its evolution under wave attack. The model consists of a parametrisation of the profile and of equations describing the evolution of parameters under any assigned wave attack. The model was developed based on a limited number of tests (both on gravel beaches and berm breakwaters) compared to the number of tests nowadays available. In the model the reshaped profile is described by the position of some characteristic points and by some slope angles, see figure 1, and for each of these variables a formula depending on the wave attack and on the initial shape, is proposed (van der Meer, 1988).
Van der Meer himself suggested possible simplifications to the model describing the variables in dependence of only two of them (van der Meer, 1994).

Dealing with deep and shallow water wave conditions, the choice of the characteristic wave height is not irrelevant.
In a previous work (Lamberti & al., 1994) was shown that a good representative wave height for the description of the reshaping phenomenon in every water condition is the $H_{2\%}$. This representative wave height was estimated for all the conditions in order to have the data as much as possible homogeneous.

Based on the availability of a large quantity of data on berm breakwater model tests, collected from European laboratories, a new model is proposed, based on a preliminary statistical multivariate analysis aiming to reduce the dimensionality of the problem in the respect to the composition principle.

2. DATA SET

In order to develop a systematic analysis of the profile parametrisation, a large number of data obtained from model tests was collected. The data sources are:

Tab. 1 Data sources

A	2D model tests from van der Meer thesis. (1988)	95 profiles of gravel beaches and berm breakwater	
B	2D model tests carried out at DHI. (1991)	307 profiles of berm breakwater	+
C	2D model tests carried out at DH.	10 profiles of berm breakwater	
D	2D model tests carried out at the University of Trondheim. (Lissev 1992).	45 profiles of berm breakwater	
E	2D model tests carried out in the facilities of Estramed Lab. (1994)	18 profiles of berm breakwater	
F	2D model tests carried out at DHI (1996)	48 profiles of berm breakwater	*
G	3D model tests carried out at the DHI. (1995)	36 profiles of berm breakwater	*
H	3D model tests carried out at the University of Trondheim. (1996)	17 profiles of berm breakwater	*
+ test performed under contract MAST-0032 * test performed under contract MAS2-CT94-0087			

Only orthogonal wave attacks are included in the database, so no longshore transport occurs and the volume of the breakwater should remain constant except for negligible phenomena of settlement.

Tests are both 2D and 3D and they were carried out for different purposes.

For the 2D test the main purpose was to investigate the influence of the wave conditions on the reshaping of the berm breakwater's trunk and, for the 3D tests, the main purpose was to study the reshaping of the roundhead and the longshore transport.

Among the 3D tests we selected only the trunk profiles, because on the head the wave attack causes a longshore transport.

Several specific purposes were pursued by the tests:

- The influence of the initial shape (berm width, berm freeboard, initial lower slope) [E],
- The influence of the permeability of the mound [F],
- The influence of the shape and permeability of the core [D],
- The scale effects [F],
- The scour protection options [F],
- The influence of the depth in front of the toe of the breakwater [H, F, E].

The berm freeboard is the elevation of the berm above the s.w.l.

All the information regarding tests is reported in a database organised as follows: the tests of each program are reported in subsequent records and the items recorded represent:

- references to the source of data,
- references to the initial profile,
- id. number of the test,
- structural parameters related to armour rock D_{n50}, D_{n15}/D_{n85}, Δ,
- parameters related to the cross section: (crest freeboard, berm freeboard (F_b), berm width (W_b), angle of structure slope), depth in front of the structure,
- parameters related to waves: $H_s, H_{2\%}, H_0, T_m, H_0T_0, s_m$ and shoaling coefficient,
- number of waves during each test and the equivalent number of waves that will be defined later,
- parameters characterising the profile after each wave attack.

A user-friendly computer application allows to see for each source the test program, the profiles and all the available information.

3. DEFINITION OF PARAMETERS

The dynamic profile is schematised by using a number of parameters (van der Meer, 1988), all of which are related to the local origin placed at the intersection between the profile and the water level. The run-up limit is described by the length l_r, the crest position by the height h_c and the length l_c, the transition to the step is described by the

height h_s and the length l_s, and the slope of the step by the angle β. In the original parametrisation, regarding gravel beaches, the step was described also by the angle γ and by the transition height h_t (see figure 1).

In the following figures some profiles, extracted from the data base, are reported as examples, and the characteristic points are located. The crest has been defined as the heights point of the profile on the berm (Fig. 2). The step as the intercept point of the tangents to the profile above and below the step, as represented in the figure 2. The angle β as the slope in the lower part of the profile. The run-up limit as the upper point where the profile differs from the profile before a wave attack (Fig. 3).

As we can notice, not all the characteristic points were recognisable in all the profiles: in fact the step develops after quite severe conditions; also the crest, which develops in the case of gravel beaches, is not always possible to be identified for the berm breakwaters.

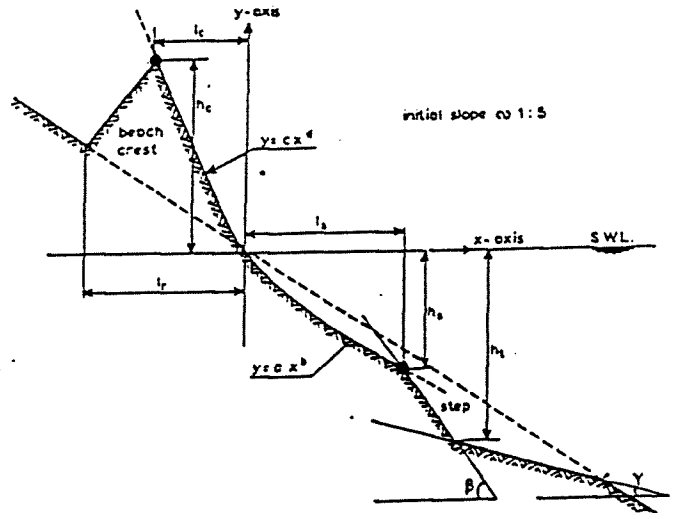

Fig. 1 Gravel beach profile parametrisation (van der Meer, 1988)

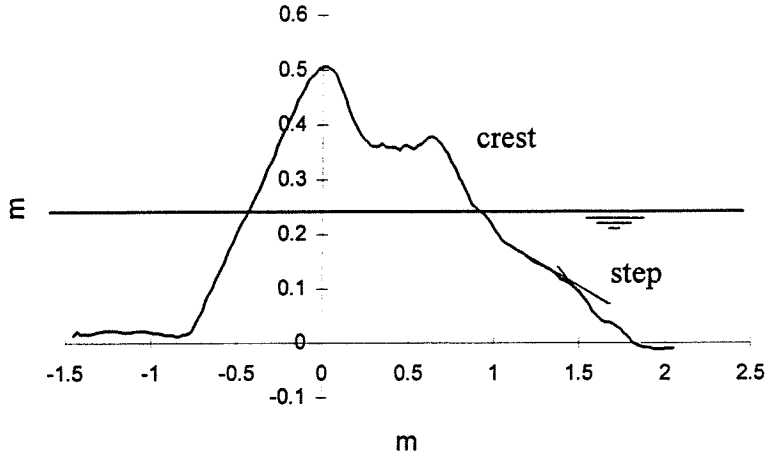

Fig. 2 Definition of berm and step

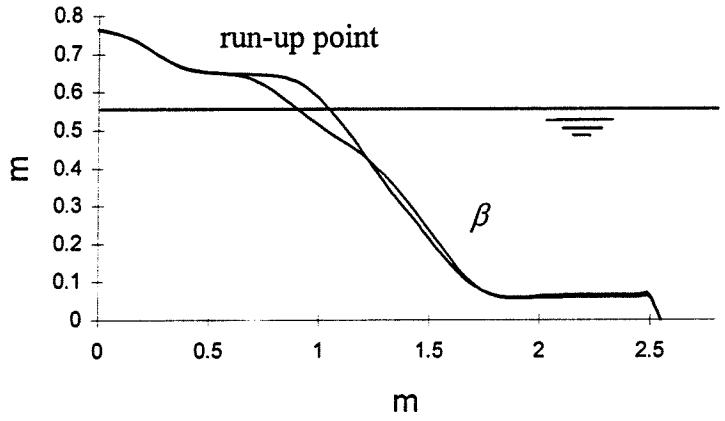

Fig. 3. Definition of the run-up point and of β

The last two parameters defined by van der Meer in the cases of gravel beaches profiles, $tg\gamma$ and h_t (Fig. 1) are not recognisable for berm breakwaters, and therefore are not taken into consideration.

4. TEST CONDITIONS

The tests analysed are very heterogeneous: the sequences of generated waves (spectra shape), the way to measure and to analyse the signals, the wave reflection analysis and the definition of wave characteristics ($H_s, T_m, \ldots etc$) are different from lab to lab. The laboratories where the tests have been carried out are very different in size, and, due to the scale effects, the results are not always easily comparable; moreover due to the subjectivity of the operator the identification of the characteristic points of each profile can also result different.

In order to homogenise the data as much as possible, all the profiles parameters were scaled with the nominal diameter. Of course some noise due to the reasons just mentioned gives a discrete margin of uncertainty to the analysis.

Not for all the tests the wave conditions in front of the breakwater are known; so to estimate the wave conditions approaching the berm breakwater placed on depth d we used the formula of Goda (1985):

$$H = \begin{cases} k_s H_0 & d/L_0 \geq 0.2 \\ min\left\{\left(\beta_0 H_0 + \beta_1 d\right), \beta_{max} H_0, k_s H_0\right\} & d/L_0 < 0.2 \end{cases} \tag{1}$$

where $min\ \{a,b,c\}$ stands for the minimum value among a, b and c, H_0 denotes the equivalent deep water height; the coefficients β_i have empirically been formulated from the numerical calculation data of random wave breaking in shallow water as follows:

$$\beta_0 = 0.028\left(H_0 / L_0\right)^{-0.38} exp\left[20 \cdot tg^{1.5}\vartheta\right]$$

$$\beta_1 = 0.51 \cdot exp\left[4.2 \cdot tg\vartheta\right]$$

$$\beta_{max} = max\left\{1.65, 0.53\left(H_0 / L_0\right)^{-0.29} exp\left[2.4 \cdot tg\vartheta\right]\right\}$$

in which $tg\vartheta$ stands for the slope of the bottom.

Previous tests (Lamberti 1994) showed that $H_{2\%}$ was the best value for the design of berm breakwater, rather than H_s, that's because only approximately 2% heights waves are responsible of the movements of the stones and consequently of the reshaping of the berm.

To determine the wave height with 2% probability, we used the approach proposed by Stive (1986), in the following equations (2) and (3). These equations give the wave height with probability 1% and 0,1% when the spectral significant wave height and the deep conditions are known.

$$H_{1^0_0} = H_{mo} \cdot (0.5 \cdot ln100)^{0.5} \cdot \left(1 + \frac{H_{mo}}{d}\right)^{-0.33} \tag{2}$$

$$H_{1^0_{00}} = H_{\mathrm{mo}} \cdot (0.5 \cdot ln1000)^{0.5} \cdot \left(1 + \frac{H_{mo}}{d}\right)^{-0.50} \tag{3}$$

Combining with the well known relation (4):

$$H_s \equiv H_{14\%} = H_{mo} \equiv 4 \cdot \sqrt{mo} \tag{4}$$

which originally derived for narrow spectra in deep water, was observed to hold even better in shallow water conditions, we obtain the following equation (5) providing wave height with only given probability:

$$H_p = H_{mo} \cdot \left(0.5 \cdot ln\ \frac{1}{p}\right)^{0.5} \cdot \left(1 + \frac{H_{mo}}{d}\right)^{-n} \tag{5}$$

where:

$$n = 0.175 \cdot \left(ln \frac{0.14}{p}\right)^{0.66} \tag{6}$$

returns the proper exponent appearing in eqs (2), (3) and (4).

The non dimensional parameters related to the waves are:

$$H_0 = \frac{H_{2\%}}{1.55 \cdot \Delta D_{n50}} \tag{7}$$

$$H_0 T_0 = \frac{H_{2\%}}{1.55 \cdot \Delta D_{n50}} \cdot \sqrt{\frac{g}{D_{n50}}} \cdot T_m \tag{8}$$

$$s_m = \frac{2\pi H_{2\%}}{1.55 \cdot g T_m^2} \tag{9}.$$

5. PRINCIPAL COMPONENT ANALYSIS

An initial, exploratory analysis was performed to give the basic statistical information concerning our data. (Tab. 2).

Tab 2- Basic Statistics

y	N. of Valid data	$\bar{y}$	Min	Max	σ_y
D_{n50} [m]	576	0.043	0.004	0.892	0.111
Δ	576	1.67	1.57	1.69	0.03
$tg\alpha$	576	0.84	0.10	1.01	0.21
D_{85} / D_{15}	224	1.60	1.25	2.25	0.26
H_0	576	4.37	0.64	29.51	3.56
s_m	576	0.040	0.014	0.067	0.010
$H_0 T_0$	576	214.3	14.3	2871.7	352.5
d / D_{n50}	576	27.84	7.78	195.12	25.48
N	576	1433	250	10000	1102
F_b / D_{n50}	495	3.75	0.90	6.22	1.36
W_b / D_{n50}	530	23.13	7.78	35.02	6.22
l_r / D_{n50}	555	20.15	1.45	353.66	35.65
h_c / D_{n50}	555	7.44	0.29	76.10	9.20
l_c / D_{n50}	555	14.22	1.45	134.15	15.81
h_s / D_{n50}	557	9.29	0.53	45.37	5.60
l_s / D_{n50}	557	33.02	2.94	243.90	26.00
$tg\beta$	572	0.68	0.11	1.43	0.26

Both freeboard and width of the berm and the characteristic parameters are scaled with D_{n50}. From now on, since all parameters are scaled with the armour stones diameter, the scaled parameters will be called with the same name as the original variables (for examples l_r / D_{n50} will be called just l_r).

It may be useful to transform the original set of variables into a new set of uncorrelated variables called principal components. These new variables are linear combinations of the original ones and are derived in decreasing order of importance so that, for instance, the first principal component accounts for as much as possible of the variance in the original data. The transformation is in fact an orthogonal rotation in a six dimension-space. The technique for finding this transformation is called Principal Component Analysis (abbreviated to PCA).

The usual objective of the analysis is to see if the first few components accounts for most of the variance in the original data. If they do, then it is argued that the effective dimensionality of the problem is less than the number of the original variables. In other words, if some of the original variables are highly correlated, they are effectively 'saying the same thing'. In this case it is hoped that the first few components will be intuitively meaningful. The PCA will simply find components which are close to the original variables but arranged in decreasing order of variance. Let's look at the correlation matrix among the 6 variables, i.e. parameters defining the limits of the active profile, ($l_r, h_c, l_c, h_s, l_s, tg\beta$): the step and the crest parameters are strongly correlated, whereas $tg\beta$ is practically uncorrelated with the other parameters (Tab. 3).

Tab. - 3 Correlation matrix among profile parameters

	l_r	h_c	l_c	h_s	l_s	$tg\beta$
l_r	1.00	0.94	0.93	0.58	0.75	-0.18
h_c	0.94	1.00	0.94	0.66	0.83	-0.15
l_c	0.93	0.94	1.00	0.60	0.78	-0.15
h_s	0.58	0.66	0.60	1.00	0.78	0.01
l_s	0.75	0.83	0.78	0.78	1.00	-0.09
$tg\beta$	-0.18	-0.15	-0.15	0.01	-0.09	1.00

Values > 0.70 are marked

The strong correlation among several variables suggests that it may be possible to extract a reduced number of independent components. So the problem consists in finding a transformation of variables into the new set of uncorrelated ones, and in the choice of the number of components to be considered in describing the phenomenon bringing the highest simplification compatible with any significant loss of information.

A preliminary standardisation of the variables was made: if y_i is the vector of the six variables, for the i[th] observation the standardised variable is $\tilde{y}_i = \frac{y_i - \bar{y}_i}{\sigma_{y_i}}$, (for instance for the variable l_r, $\tilde{l}_r = \frac{l_r - \bar{l}_r}{\sigma_{l_r}}$).

Formally the transformation from the 6 variables $\tilde{y}_i$ to the components $\tilde{f}_i$ is the matrix product: $\tilde{f}_i = A \cdot \tilde{y}_i$ and for all the observations:

$$F = A \cdot Y \tag{10}$$

where F is the matrix of the components (dimension 6xn, n number of the observations) and Y is the matrix of the standardised variables. A is the factor scores matrix, the orthogonal matrix of transformation from variables to components. The A matrix (for our data) is given in table 4.

For instance eq. 10 with regards to the first component is:

$$\tilde{f}_1 = a_{11} \cdot \frac{h_r - \overline{h}_r}{\sigma_{h_r}} + a_{12} \cdot \frac{h_c - \overline{h}_c}{\sigma_{h_c}} + a_{13} \cdot \frac{l_c - \overline{l}_c}{\sigma_{l_c}} + a_{14} \cdot \frac{h_s - \overline{h}_s}{\sigma_{h_s}} + a_{15} \cdot \frac{l_s - \overline{l}_s}{\sigma_{l_s}} + a_{16} \cdot \frac{tg\beta - \overline{tg\beta}}{\sigma_{h_r}} \quad (11).$$

Tab 4. - Matrix *A* of Factor Scores

	f_1	f_2	f_3	f_4	f_5	f_6
l_r	0.22	-0.09	-0.51	-0.61	-2.41	-2.04
h_c	0.23	-0.02	-0.31	-0.02	-0.28	4.11
l_c	0.23	-0.05	-0.45	-0.24	2.88	-1.40
h_s	0.19	0.26	0.98	-1.25	0.10	-0.07
l_s	0.22	0.11	0.41	1.97	-0.32	-0.80
$tg\beta$	-0.04	0.94	-0.39	0.04	-0.07	-0.06

From the inverse transformation:

$$Y = A^{-1} \cdot F = B \cdot F \quad (12)$$

it is possible to obtain again the original standardised variables, when the components are known.

The matrix B of the factor loadings is the inverse matrix of A; the factor loadings express the correlation between the components and each variable. The components are arranged in decreasing order of explained variance, given in the last line of the table.

Tab. 5 Matrix B^T of Factor Loadings

	f_1	f_2	f_3	f_4	f_5	f_6
l_r	0.93	-0.09	-0.27	-0.10	-0.17	-0.09
h_c	0.97	-0.02	-0.17	0.00	-0.02	0.17
l_c	0.94	-0.05	-0.24	-0.04	0.20	-0.06
h_s	0.78	0.26	0.53	-0.21	0.01	0.00
l_s	0.91	0.11	0.22	0.34	-0.02	-0.03
$tg\beta$	-0.17	0.96	-0.21	0.01	0.00	0.00
Expl.Var	0.69	0.17	0.09	0.03	0.01	0.01

Loadings > 0.70 are marked

The first component is highly and positively correlated to the five lengths describing the profile, so the component, that alone describes the 69% of the variance, is representative of how much the profile reshapes. This attribution is very important, as will be seen later, because using the first component as indicative of the damage suffered, the concept of equivalent number of waves was introduced.

The second component changes as the slope of the step, and is also function of the depth of the water in front of the breakwater. In the second and the third components is evident the different behaviour of the upper part of the profile (described by the run-up and the crest) from the lower (described by the step and the slope).

The 1st with the 2nd and the 3rd component describe 95% of the variance so the following analysis is performed with only these components; due to the independence of the components, this can operatively be done substituting the mean value 0 to the unrepresented components, i.e. truncating the loading matrix to the first three columns. Obviously when we neglect the contribution of the last three components, in the estimations of the variables (the geometric parameters) from the components (eq. 12) the result will lose in precision. This is shown in fig. 5 referring, for instance, to the parameter h_c. The loss is represented in the figure by the scatter of the data: on the abscissa are the

original standardised parameters and on the ordinate the estimated ones through eq. 12 based on three components.

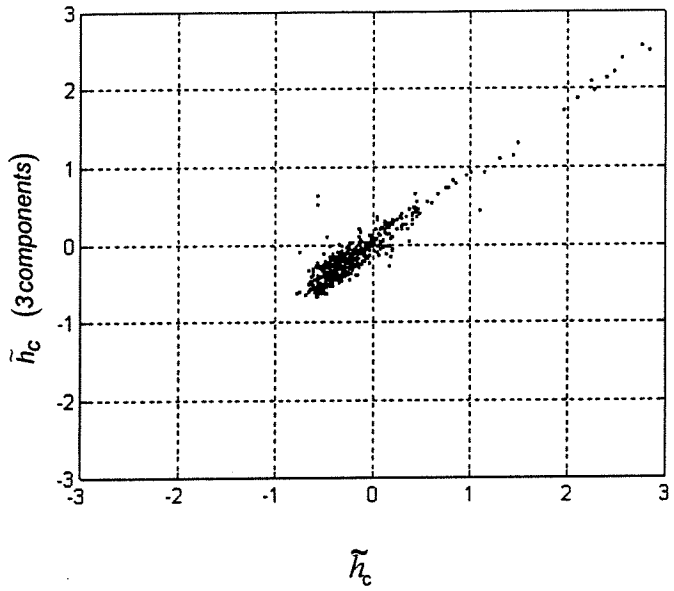

Fig. 4- $\tilde{h}_c$ given by eq. 12 when only 3 components are taken into account

The next three figures point out the contribution of each component: the two represented profiles of the breakwater represented values -1 and +1 of the specific component, all the others being set to 0 (average conditions).

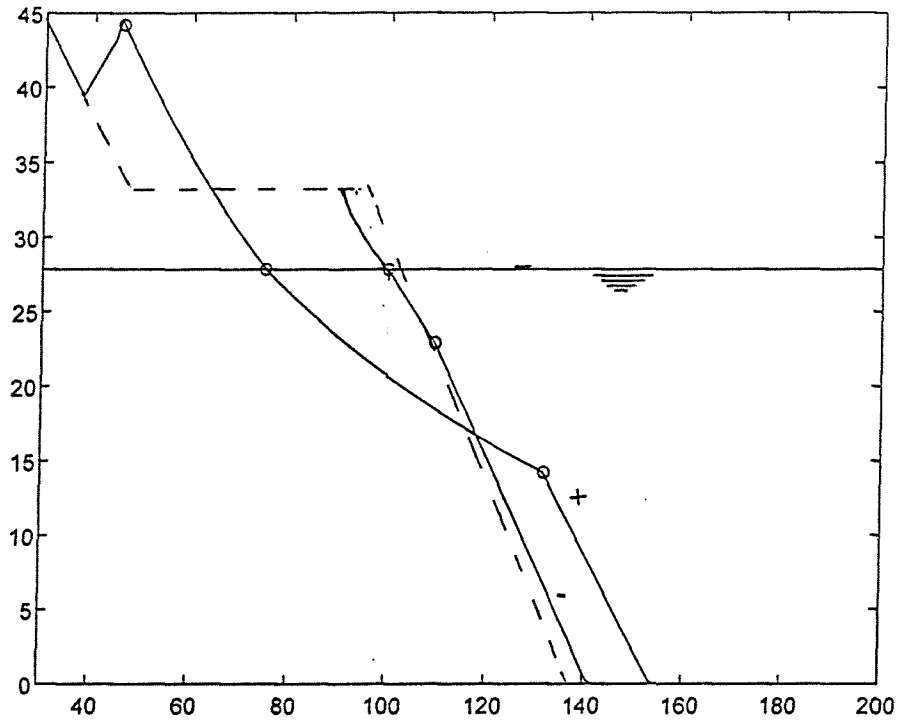

Fig. 5 Effect of the 1st component on the berm breakwater profile

In figure 5 the initial shape is also drawn (the dimensions of the built breakwater are the average on the data set). The -1 profile describes a very weakly reshaped breakwater and the +1, in the opposite direction a very severely reshaped or damaged. It is evident that the first component is a measure of the general reshaping and erosion process.

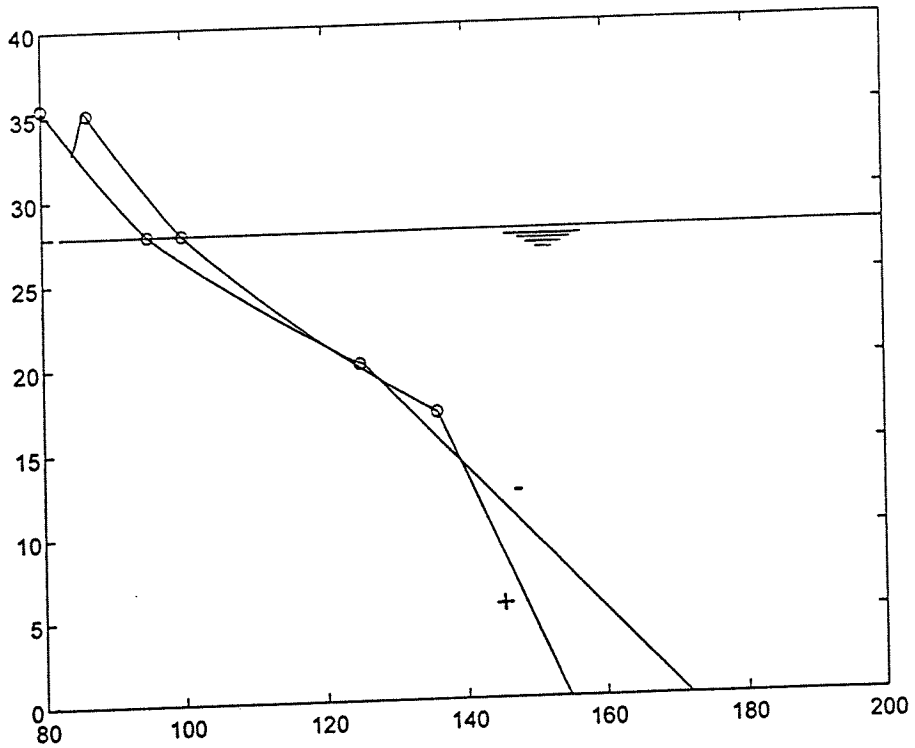

Fig 6. Effect of the 2nd component on the berm breakwater profile

In figure 6 is evident the contribution of the second component: mainly the slope of the step changes. Increasing the component the slope decreases and vice-versa. As the component increases the step becomes more prominent.

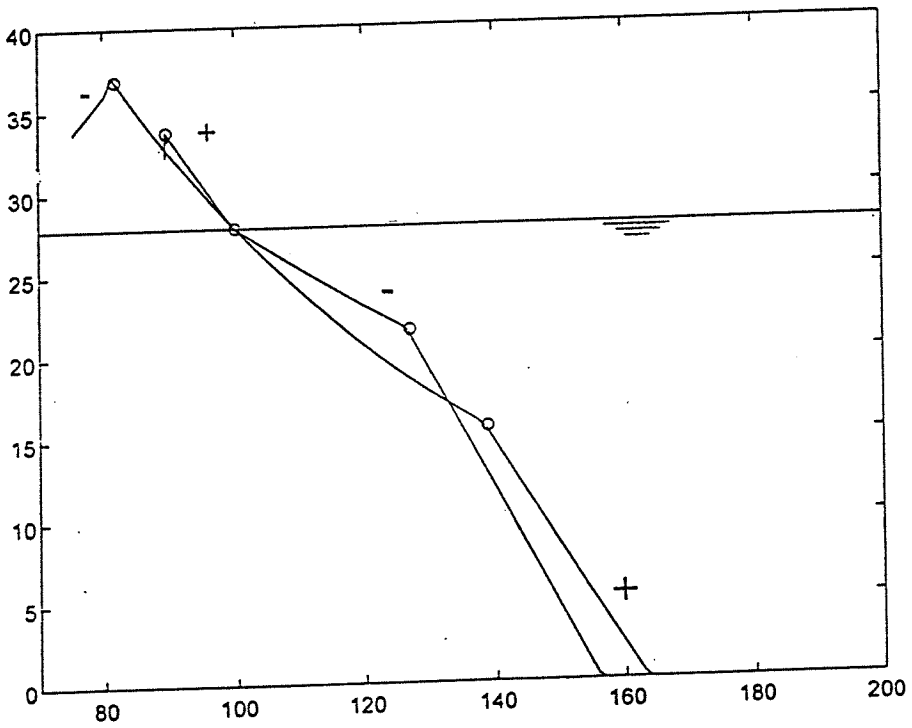

Fig. 7. Effect of the 3rd component on the berm breakwater profile

Figure 7 represents the effect of the 3rd component. As it increases the extension of the part of the active profile below the water level increases, and the part above decreases. This component is indicative of the asymmetry of the active profile.

Keeping the relevant dimensionality of the phenomenon fixed to three, an extraction of components with a varimax normalised rotation was performed. This means that a rotation of the normalised factor loadings (raw factor loadings divided by the square roots of the respective communalities) was performed aiming at maximising the variances of the squared normalised factor loadings across variables for each factor (Tab. 6); in other words the rotation aims at obtaining factor loadings as much as possible close to 0 or ± 1 in order to have the greatest possible contrast among the components.

Tab. 6 Factor Loadings (Varimax rotated)

	f_1	f_2	f_3
l_r	0.93	0.10	0.27
h_c	0.90	0.07	0.40
l_c	0.92	0.07	0.32
h_s	0.32	-0.03	0.92
l_s	0.61	0.04	0.71
$tg\beta$	-0.09	0.99	0.01
Expl.Var	0.50	0.17	0.28

Loadings >0.7 are marked

The parameters describing the two parts of the structure (above and below the s.w.l.) are in this way more distinct than from the PC decomposition. The first component however describes now only the 50% of the variance and the variance explained by the third is now increased to 28%. These components do not allow anymore the description of the greatest part of the phenomenon of the reshaping by only one factor.

Therefore in the following analysis the performed PC decomposition (Tab. 5) was used and only the first three components were taken into account.

In order to investigate the sensibility of the phenomenon to the initial shape of the profile, a preliminary analysis was performed: the factor loadings were extracted for sub set of data regarding the profiles still having memory of the initial shape.

This means that the analysis was repeated for sub - sets of data characterised by:

- defined range of berm freeboard, (in order to investigate the influence of the freeboard)

- defined range of berm width (in order to investigate the influence of the width)

and the analysis was conducted also for the only cases of profiles which didn't have any memory of the initial profile, (this means the profiles for which the berm was still recognisable).

For these subset the correspondence variables-components is the same as described in tab. 5, of course the scores and factors are not exactly the same.

The conclusion of the multivariate analysis (Principal Component method) is that the variables describing the phenomenon can be reduced to three. The first component is strongly correlated to the size of the active profile, and the second to the protruding of the step, and the third to the extension asymmetry of the parts above and below the free surface. The first component alone represents the general erosion process of the berm.

6. MODEL FOR THE 3 COMPONENTS

The damage suffered from the breakwater during a storm depends on its duration and intensity. In the database the duration of each test is described by the number of waves, but this information represent the effect of antecedent wave attacks. So it was necessary to estimate a kind of equivalent number of waves responsible for the reshaping. In fact erosion of the structure is due primarily not only to the waves of the last storm (in laboratory of the last test) but also to the previous storms, which have modelled the breakwater in the past, even if by testing with increasing wave intensity the effect of the last is usually dominant.

The effect of the antecedent wave attacks may be, with some approximation, thought as equivalent to a longer duration of the current attack, in the sense that the final damages are as similar as possible.

Since the phenomenon is multidimensional a complete equivalence is not generally

possible; we start by assuming the equivalence relative to the 1st component representing the most relevant aspect of the damaging process.

A preliminary correlation analysis showed which environmental parameters the components depend on.

The first component is well correlated to the intensity of waves (H_0 and s_m) and to the duration of the waves attack through a power law as van der Meer suggests (1988).

The model applied to describe how the first component depends on the wave conditions is:

$$f_1 = cost \cdot H_o^{\ a} \cdot N_e^{\ b} \cdot s_m^{\ c} \tag{13}$$

$$f_1 = \tilde{f}_1 + k_1 \tag{14}$$

$$k_1 = a_{11} \cdot \frac{\overline{h}_r}{\sigma_{h_r}} + a_{12} \cdot \frac{\overline{h}_c}{\sigma_{h_c}} + a_{13} \cdot \frac{\overline{l}_c}{\sigma_{l_c}} + a_{14} \cdot \frac{\overline{h}_s}{\sigma_{h_s}} + a_{15} \cdot \frac{\overline{l}_s}{\sigma_{l_s}} + a_{16} \cdot \frac{\overline{tg\beta}}{\sigma_{h_r}}$$

To calibrate the model we used the tests in which the number of equivalent waves is known: the tests in which the intensity of the waves (H_0 and s_m) remains constant during all the tests sequence.

At the end of the first wave attack the equivalent number and the real number of wave is the same $N_1 = N_{e1}$.

Due to the change in wave intensity at the beginning of the second attack the previous history can be assimilated to N_{e2} waves of current intensity given by:

$$H_{01}^{\ a} \cdot N_{e1}^{\ b} \cdot s_{m1}^{\ c} = H_{02}^{\ a} \cdot N_{e2}^{\ b} \cdot s_{m2}^{\ c}$$

i.e.

$$N_{e2} = \left(\frac{H_{01}}{H_{02}}\right)^{16} \cdot \left(\frac{s_{m1}}{s_{m2}}\right)^{-2} \cdot N_{e1} \tag{15}$$

At the end of the wave attack the number of waves is increased by N_2: $N_{e2} = N_{e2} + N_2$ and so on for every attack in the wave series. In this way every profile was associated to a wave attack having an actual and an equivalent number of waves. In the figure 8 there is an

example of computation of the equivalent number of waves during a sequence of tests of increasing intensity. Each test lasts 2000 waves.

The regression was repeated using all the data available and the equivalent number of waves obtaining slightly different regression coefficients.

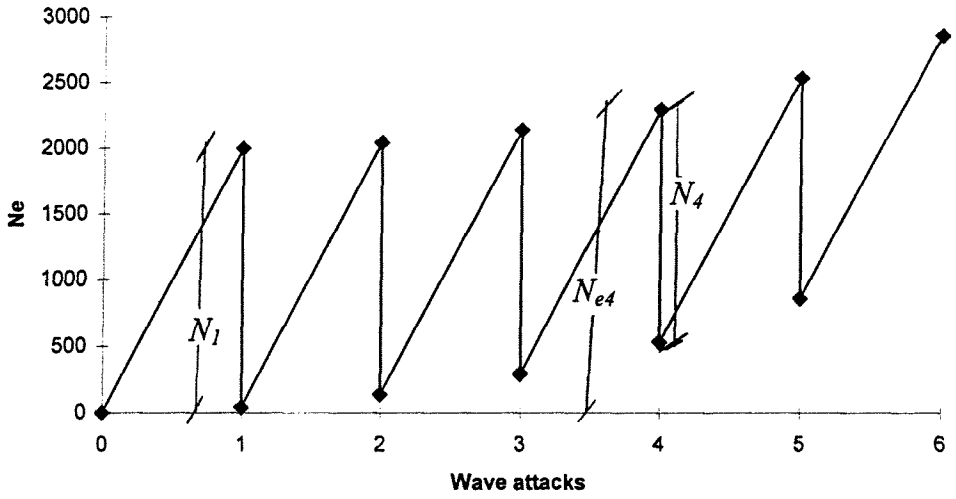

Fig. 8 Equivalent numbers of waves

As we formulated a model for the component 1 depending on the environmental and structural conditions, we did for the components 2 and 3:

$$\tilde{f}_1 = 0.041 \cdot H_0^{1.08} \cdot N_{eq}^{0.05} \cdot s_m^{0,17} - 1 \tag{16}$$

$$\tilde{f}_2 = 2.441 + 0.805 \cdot ln(d) - 0.46 \cdot ln(H_0) - 2.96 \tag{17}$$

$$\tilde{f}_3 = \frac{(-0.15 + 0.025 \cdot H_0)}{(0.28 + 0.37 \cdot ctg\alpha)} - 0.16 \tag{18}$$

the first component depends on the waves intensities, the second (that is so highly correlated to the $tg\beta$) depends on the wave height and on the depth at the toe of the breakwater and the third depends on the initial slope and on the waves intensity.

Once the 3 components are calculated, through eq.13 it is possible to estimate the 6 original variables.

Fortunately the second and the third components showed not to depend evidently from the wave attack duration, providing more confidence on the equivalent duration we defined.

Since the second and the third component depend on wave intensity, the model does not satisfy the principle of continuos dependence on time (corollary of the composition principle). I.e. when wave intensity is increased abruptly components 2 and 3 respond instantaneously to the increased wave intensity, that is not reasonable.

Our equations are based on experience drawn from wave attacks during at least waves and waves on average, and should not be applied to attacks significantly shorter than the average duration.

In the following figure 9 to 14 are the six parameters computed from the model compared with experimental data. On the axis are the parameters in dimensional form.

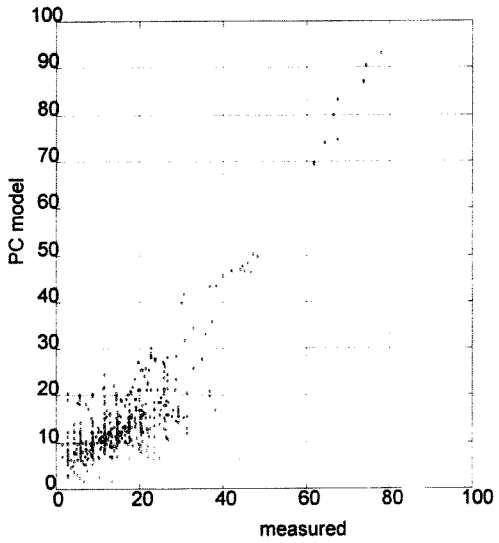

Fig. 9 l_r from the components model

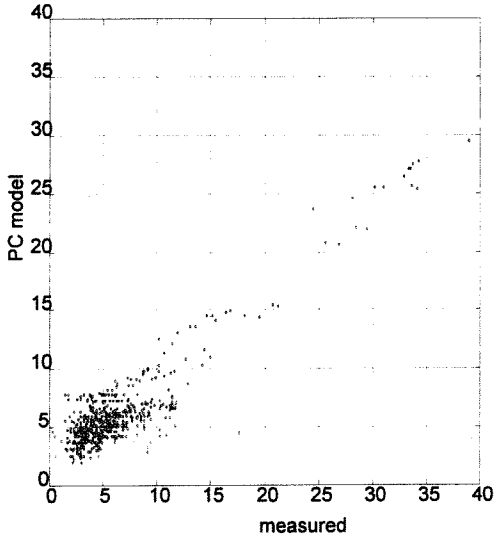

Fig. 10 h_c from the components model

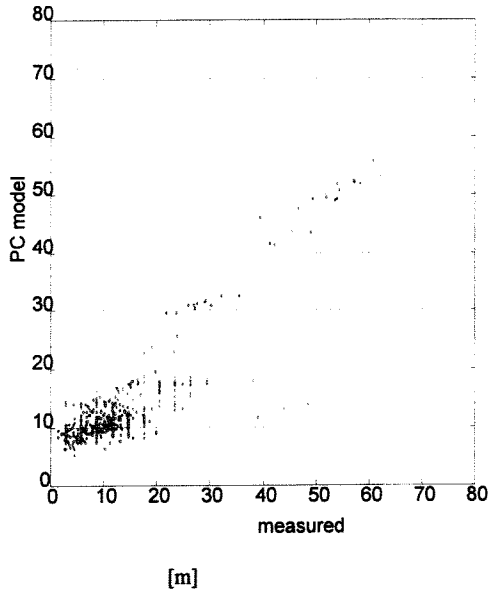

Fig. 11 l_c from the components model

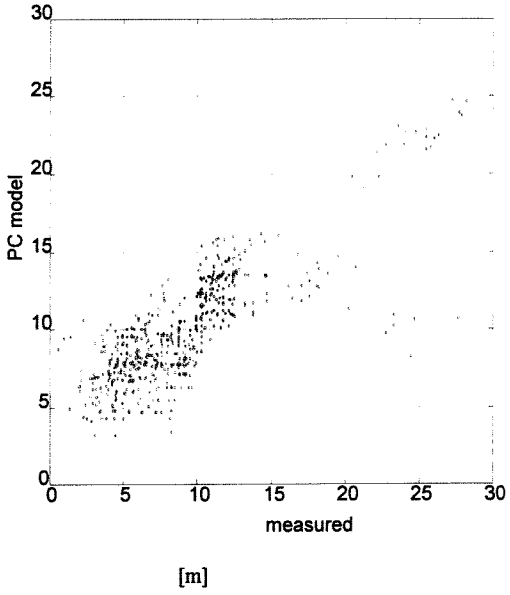

Fig. 12 h_s from the components model

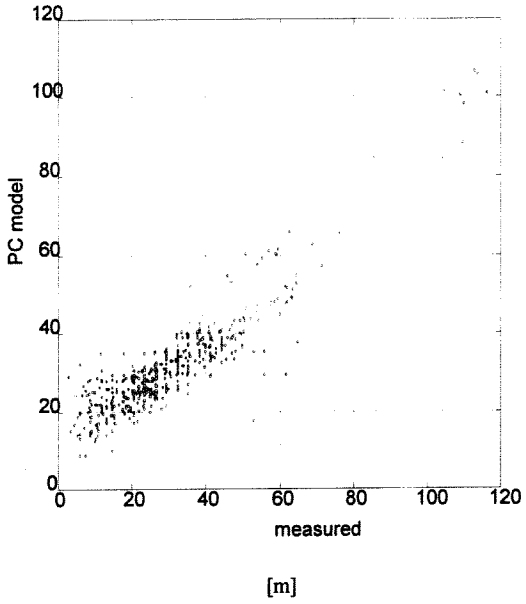

Fig. 13 l_s from the components model

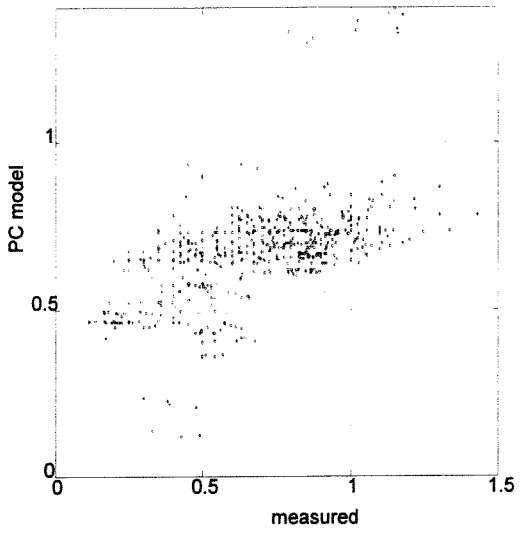

Fig. 14 $tg\beta$ from the components model

The model is satisfactory concerning the lengths parameter, contrarily the slope of the step ($tg\beta$) is not so well described. In tab. 7 the basic statistic of the measured and of the estimated $tg\beta$ are compared.

Tab. 7. Statistics on the estimated $tg\beta$

	Mean	Min	Max	σ
measured	0.68	0.11	1.43	0.26
estimated	0.66	0.11	1.39	0.15

The mean and the range of the estimated variable are similar, but standard deviation of the estimated $tg\beta$ is low, so the model underestimates the value of $tg\beta$.

In many situations the profile near the step point is rounded and the slope below the step is sharp. In these cases the parameter itself is poorly defined and its experimental estimate is probably subjects to relevant errors. The $tg\beta$ probably depends on the shape of the stones of the mound, but this information is not systematically available.

7. COMPARISON OF THE PROPOSED MODEL WITH EXPERIMENTAL DATA AND OTHER EXISTING MODEL

Once the equivalent number of waves is estimated the three components and the six parameters after each wave attack are computed, the profile can be drawn, the horizontal position being defined by the conservation of the volume under the profile.

The line joining the crest to the still water level and to the step is a power function (Vellinga, 1986), and the line describing the profile from the step is a straight line with slope β. Once the profile was drawn, was translated from the run-up abscissa in the horizontal direction, in order to keep the initial volume constant, because no longshore transport occurs during head on wave attack.

The profiles were compared with the output profiles of BREAKWAT©, the software developed by Delft Hydraulics from the van der Meer's equations.
The model proposed by Van der Meer gives the equations to estimate the parameters of the profiles. These equations are independent, even if the form is very similar. The dependence of the previous profile is given by the terms, $cotg\alpha_1, cotg\alpha_2, cotg\alpha_3$ (Fig. 15, van der Meer, 1988).

The software is able to show how the profile of a berm breakwater or gravel beaches reshapes under given sequences of wave attack in nearly all the design conditions. In fact the software doesn't give any answer when the damage is low, when the slope is steep and when the water depth is limited. These limitations are due to the fact that in these conditions the outputs are less reliable and these advises suggest that the tested conditions are not the conventional.

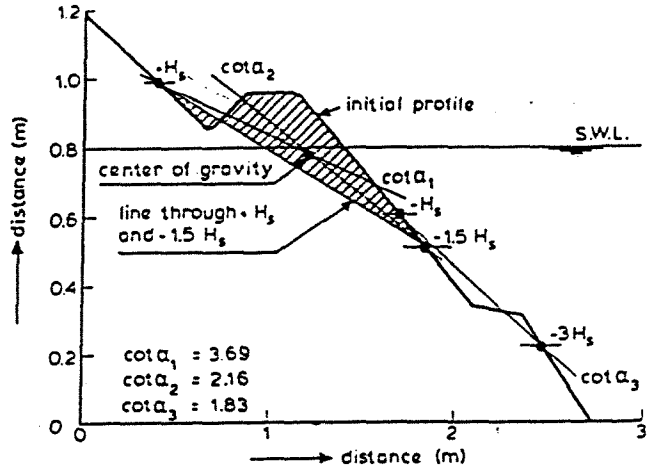

Fig. 15 Definition of $cotg\alpha_1, cotg\alpha_2, cotg\alpha_3$

The results of the reshaping of the breakwater from the model compared with the experimental profiles are proposed as example regarding the test series run at the DHI in 1995 on a 3 D model (source G). The initial profile is shown in Fig. 16.

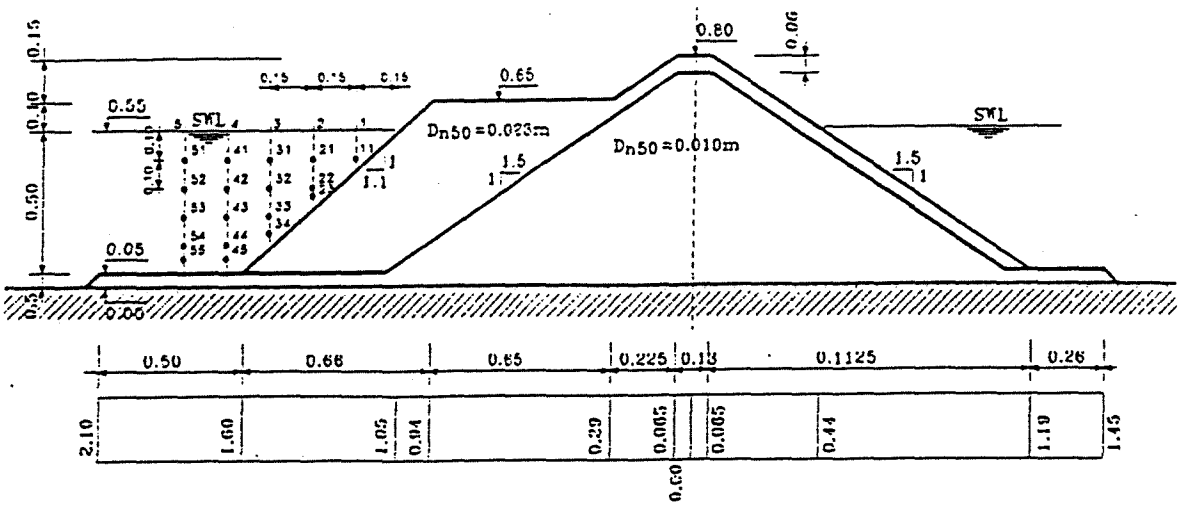

Fig. 16 Initial profile

The test program carried out was a sequence of six wave attacks in increasing intensity with a duration of 2000 waves (Tab. 8).

Tab. 8 Test Program

H_s [m]	T_m [s]	s_m	*depth* [m]	D_{n50} [m]
0.058	0.864	0.05	0.55	0.023
0.078	0.998	0.05	0.55	0.023
0.097	1.116	0.05	0.55	0.023
0.117	1.222	0.05	0.55	0.023
0.136	1.32	0.05	0.55	0.023
0.155	1.412	0.05	0.55	0.023

For the attack 1 to 4 (stability number from 1.5 to 3) BREAKWAT© doesn't give any result because the mobility is suggested to be too low. Of course the equations proposed by van der Meer give results for any structure and wave conditions. In the following figure is shown for the attack 1-4 the reconstructed profiles using the principal components model and the measured profiles. For the last two tests also the output of BREAKWAT© (in dash line) is compared.

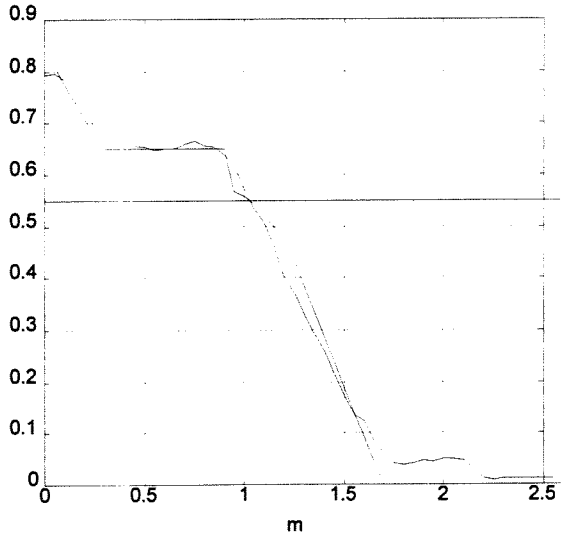
0.9
0.8
0.7
0.6
0.5
0.4
0.3
0.2
0.1
0
0
0.5
1
1.5
2
2.5
m

a) $H_0 = 1.5$

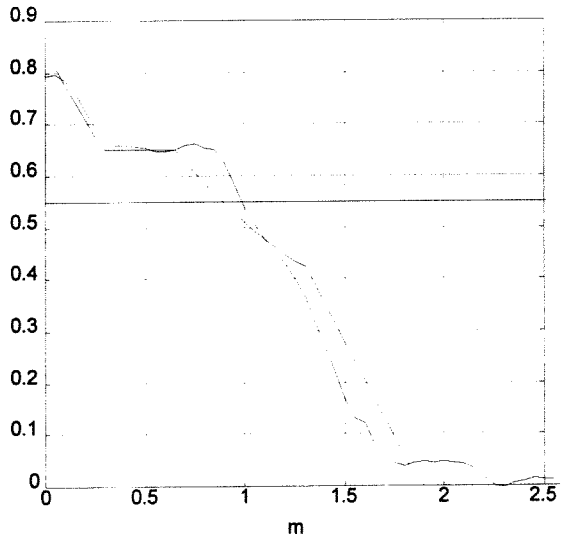
0.9
0.8
0.7
0.6
0.5
0.4
0.3
0.2
0.1
0
0
0.5
1
1.5
2
2.5
m

b) $H_0 = 2.0$

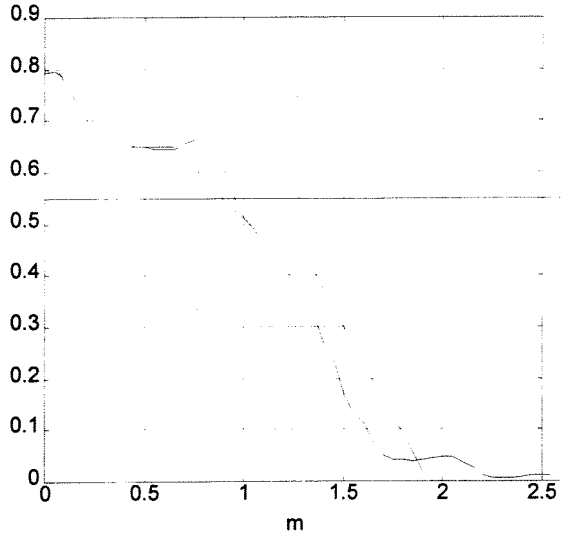
0.9
0.8
0.7
0.6
0.5
0.4
0.3
0.2
0.1
0
0
0.5
1
1.5
2
2.5
m

c) $H_0 = 2.5$

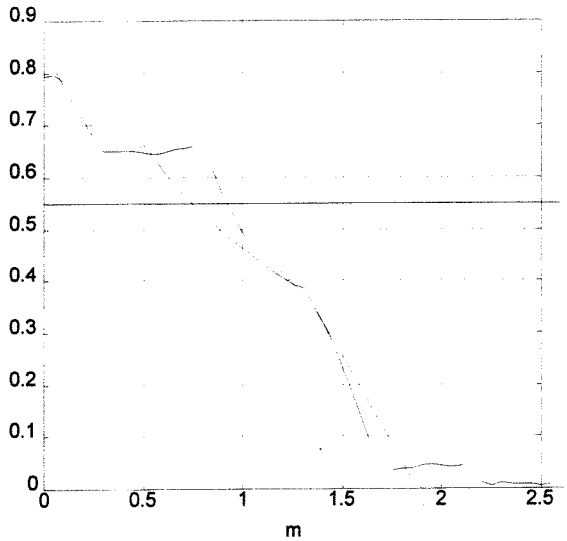
0.9
0.8
0.7
0.6
0.5
0.4
0.3
0.2
0.1
0
0
0.5
1
1.5
2
2.5
m

d) $H_0 = 3.0$

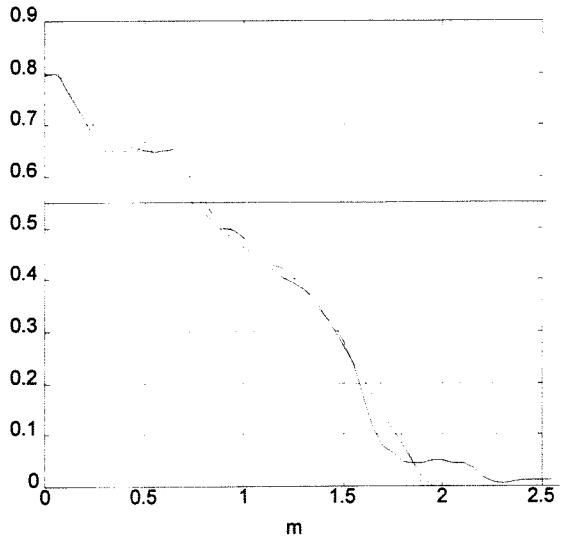

e) $H_0 = 3.5$

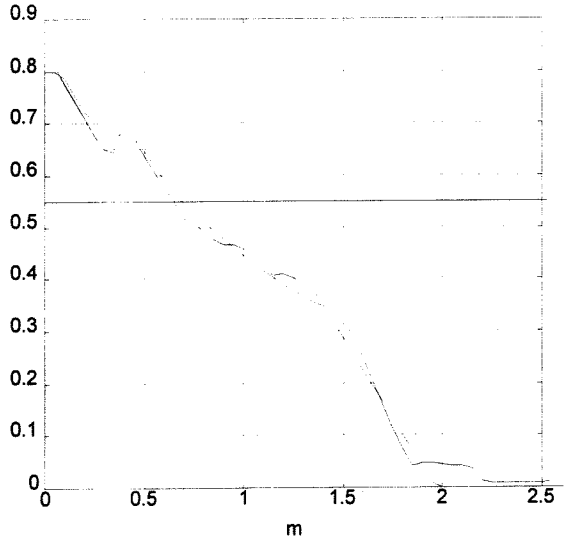

f) $H_0 = 4.0$

Fig. 17. Comparison between the measured profiles and the models, BREAKWAT© results in dash line

The principal component model output is satisfactory for low damage (Fig. 17-a Fig. 17-b) and for great damage, when an equilibrium is reached (Fig. 17-e Fig. 17-f); in the intermediate cases the model gives as result a greater damage than in reality (Fig. 17-c Fig. 17-d).

The comparison between the output of the three components model and the measured profiles was also carried out for the test series from source D. The results confirm the conclusions found.

The influence of the initial shape of the profile was investigated, in order to propose a dependence of the model from the initial shape parameters, but a trend able to explain the behaviour when the equilibrium is not already reached was not found.

8 CONCLUSIONS

The reshaped profile is described by a set of six parameters, which through a multivariate principal component analysis is transformed into a set of six components of decreasing explained variance. The first three describe 95% of the variance in our data set.

The first component represents the general erosion process and is function of the intensity of the wave attack; the second is highly correlated to the slope of the step and is function mostly of the depth at the toe; the third, which describes (together with the second) the difference from the two parts of the active profile, above and under the s.w.l., is function of the initial slope and of the intensity of the wave attack.

The model predicts the evolution of the profiles under a sequence of wave attack in respect of the composition principle only according to the first component. The model predicts accurately the equilibrium profile, when the memory of the initial profile is lost: in cases in which the berm still exists and is wide, the proposed model do not describe the dependence from the shape of the initial profile and it overestimates the damage for modest wave attack.

Acknowledgements

The present study was partially supported by the research and technological development programme in the field of Marine Science and Technology (MAST) financed by the European Union, Contract MAS2-CT94-0087.

References

Ahrens J.P. (1987). Characteristics of reef breakwaters. CERC, Vicksburg, Technical Report CERC-87-17.

Archetti R., Lamberti A., Tomasicchio G.R. (1995). *Reshaping Breakwater: longshore transport and recession of the berm.* 2nd Workshop on Berm Breakwater Structures 6 Oct. 1995. London.

Archetti R. Lamberti A. (1996). *Parametrizzazione del profilo di frangiflutti a berma.* IV Congresso AIOM, 3-5 ott. 1996 Padova Italy.

Archetti R., Lamberti A. (1996). *Reshaping Breakwater: profile parametrisation.* 3rd Workshop on Berm Breakwater Structures. 10-11 May 1996. Stavanger.

Chetfied C., Collins A.J. (1983). *Introduction to multivariate analysis.* Chapman & Hall.

CIRIA - CUR, (1991). *Manual on the use of rock in coastal and shoreline engineering.* CIRIA, London, Special publication 83 - CUR, Gouda, Report 154.

Dassonvilles P. (1993). *Introduction a l'analyse factorielle.* Ecole Européenne des Affaires.

DH (1994). BREAKWAT USER'S MANUAL. Version 2.01.

Goda Y. (1985). *Random Seas Waves and Design of Maritime Structures.* University of Tokyo Press.

Hall K.R., Kao J., Mulcahy M., (1991). *The influence of armour stone gradation on dynamically stable breakwaters.* Coastal structures and breakwaters, 6-8-Nov. 1991, London.

Lamberti A , Tomasicchio G.R., Guiducci F. (1994). *Reshaping breakwaters in deep and shallow water conditions.* XXIV Int. Conf. Coastal Eng., Kobe, Japan 1994.

Tomasicchio G.R., Lamberti A., Guiducci F. (1994). *Stone movement on a reshaped profile.* Proc. XXIV Int. Conf. on Coastal Eng., Kobe, Japan.

Van der Meer J.W. (1988). *Rock Slopes and Gravel beaches under wave attack.* TUD Ph.D. thesis.

Van der Meer J.W. (1994). *Conceptual design of berm breakwaters,* Proc. Hornafjordur International Coastal Symposium. 20-24 June, 1994 Iceland.

Vellinga P. (1986). *Beach and dune erosion during storm surges.* TUD Ph.D. thesis.

Stive M.J.F. (1985). *Extreme shallow water wave conditions.* DH int. report H533.

Irregular wave induced forces on armor unit on berm breakwaters.

Ketil Westeren[1] and Alf Tørum[2]

Abstract

An experimental study has been carried out on the forces from irregular waves on a single armor unit at different locations along a berm breakwater slope. The results show that the wave forces are largest above the still water line. The results helps to understand some of the complex mechanisms for the reshaping of the berm.

Introduction

It is the water velocity field on a breakwater front that is the main governing factor with respect to the stability of armor cover blocks. This velocity field and the forces have been poorly known. The different formulas for cover block weight (Iribarren 1938; Hudson 1958; Hedar 1960) have been based on some approximate concept on the velocity and the forces induced on the individual blocks, leading to formulas with a single unknown coefficient. The value of this coefficient has been determined from model tests.

The forces on different blocks have been expressed as a Morison force formulation, Morison et al (1953). It is not precisely known which velocities and C_D, C_M and C_L values, etc. should be applied in the equation since breakwater cover blocks are embedded among each other and the flow is between as well as over and under cover blocks.

One of the first attempts to calculate the velocities for downrush on a rubble mound breakwater slope was made by Brandtzæg and Tørum (1966) and by Brandtzæg et al. (1968). They measured velocities with a micropropeller. There was fair agreement between the measurements and the simple mathematical model that was derived to calculate the velocities.

Sawaragi et al. (1982) measured particle velocities on the breakwater slope by filming particles made of sponge, with the same specific mass as water, introduced in the water. The point-to-point movement of the particles was recorded on 16 mm colour film taken by a high speed camera (50 frames per second). From the film, the particle velocities were obtained by superposition of projected film frames to give a distance and a time interval of movement. Sawaragi et al (1982) found that the non-dimensional maximum velocity was a function of the surf similarity parameter and the ratio of wave height and the water depth. Sawaragi et al (1982) did not compare the velocity measurements with any theoretical results.

Kobayashi et al. (1986, 1987) and Kobayashi and Wurjanto (1989) developed a numerical model for the computation of the water-particle velocities on an impervious rubble mound slope.

---

[1]Norwegian University of Science and Technology (NTNU), Division of Structural Engineering, 7034 Trondheim, Norway.
[2]NTNU/SINTEF Civil and Environmental Engineering, 7034 Trondheim, Norway.

Breteler and van der Meer (1990) report the measurement and computation of wave induced velocities on a smooth slope.

Tørum and van Gent (1992) obtained results from water particle velocity measurements with a laser Doppler velocimeter on a berm breakwater. They compared the results with the computer program ODIFLOCS (van Gent 1992) based on modification of the long wave theory. There was a fair agreement between the measured and calculated velocities.

van Gent (1993a) obtained similar results from water particle velocity measurements with an electromagnetic current meter. The comparison between the measured and the calculated velocities with the computer program ODIFLOCS was fair. van Gent et al (1994) used the physical model test results on water particle velocities obtained by van Gent (1993a) to compare the results obtained with the two dimensional computer program SKYLLA. This computer programs has been developed to calculate the flow on and in rubble mound breakwaters, dikes etc., van der Meer et al (1992).

Other computer programs have also been developed and which can be used for calculating waves on slopes, e.g. SYSTEM 3xy, Fisher et al (1992).

The interior flow in a breakwater is a flow in a porous medium. Hence the flow inside the breakwater is described by equations valid for flow in porous media.

The flow in porous media is in principle more complicated than a free flow. One does not know exactly the flow in the pores between the grains nor the resistance of the flow by the grains. Much research has been carried out on the flow in porous media for stationary flow. It seems that the so-called Forchheimer equation, Forchheimer (1901), is presently generally accepted as the governing equation for the steady turbulent flow in porous media. For non-stationary turbulent flow in porous media, like the flow in the berm of a berm breakwater, the extended Forchheimer equation, extended by an unsteady flow term, is frequently used. The discussions have mainly been on the mathematical formulations of the coefficients in the equations and the numerical values of the coefficients.

During the European Commission research program on coastal structures under the Marine Science and Technology program (EU MAST I and II - Coastal Structures) fairly large scale experiments in an oscillation water tunnel were carried out to arrive at proper values of the coefficients in the Forchheimer equation to be used for breakwaters, Andersen et al (1993), van Gent (1993b), Andersen (1994), van Gent (1995).

The wave forces on the individual armor unit is ultimately the governing factor for the stability of a breakwater. The wave forces on a single armor unit embedded among other units on the front of a breakwater are however not exactly known. There have been some attempts to measure these forces.

Sigurdson (1962) measured forces from regular waves on spheres mounted together to form an idealised breakwater slope. No water particle velocities were measured. Sigurdson's measurements showed clearly the complexity of the wave forces on a single armor unit. Sandstrøm (1973) carried out similar tests.

Jensen and Juhl (1988, 1990) carried out tests on a two-dimensional (2D) breakwater structure consisting of horizontal cylinders. They measured the forces on individual cylinders and the run-up and run-down of the waves on the breakwater slope. No measurements of water particle velocities were carried out.

Sakakiyama and Kajima (1990) measured the wave forces on a concrete armour unit and the run-up and run-down of the waves on the breakwater slope. No measurements of the water particle velocities were carried out.

Losada et al (1988) measured the forces under solitary waves on a cubic block close to a flat bottom. The block was a single block and not surrounded by other blocks. They analysed the forces in view of the Morison force formulation and obtained instantaneous as well as average C_D, C_M and C_L values based on water particle velocities and accelerations obtained from the solitary wave theory.

Iwata et al (1985) carried out an experimental study on the wave forces on a single armor unit on a two-layer rubble mound slope with uniform slopes 1:2 and 1:3. The measurements included water particle velocity measurements just above the force-sensing rubble. The rubble used in the experiments was composed of round rubble with diameters D = 0.015 and 0.022 m. The forces parallel to the slope were, among other items, analysed according to the Morison force formulation and drag and inertia force coefficients were obtained.

Rufin et al (1994) measured the wave forces on a non-embedded armor unit of a submerged wide crown breakwater and analysed the results in view of the Morison force formulation.

Tørum (1992, 1994) carried out laboratory measurements on wave forces on an embedded single armor unit on a berm breakwater. Tørum measured also water particle velocities with a laser Doppler velocity meter and analysed the results in view of the Morison force formulation. Both forces and velocities were measured parallel and normal to the breakwater slope.

Cornett and Mansard (1994) measured the shear stress and the normal stress on the surface layer of a rubble mound breakwater. The conclusion they arrived at was that the maximum and minimum stresses may be reasonably estimated by using friction coefficients obtain in turbulent oscillatory flow over rough surfaces.

All the referenced work on wave forces on single armor units has concentrated on forces in regular waves. It was thus felt that there was a need to investigate the wave forces on individual armor units in irregular waves for armor units placed at different locations along the slope of a berm breakwater. Hence we undertook an experimental study on this subject.

Test set-up and measurement systems.

Wave flume and berm breakwater model.

The test set-up was essentially the same as used by Tørum (1992, 1994).
The wave flume with the berm breakwater model is shown in Figure 1. The flume is 1 m wide and 33 m long. The breakwater cross section is shown in Figure 2. The nominal stone diameter is defined as $D_n = (W/\rho_s)^{1/3}$, W = weight of a stone (in air), ρ_s = specific mass of the stones. The "diameter" D_n is thus equivalent to the edge of a cube with the same mass as the irregular shaped armor unit. This diameter definition, first introduced by van der Meer (1988), is now frequently used in breakwater design and research work.

W_{50} = 50 % of the stones have a larger (or smaller) mass than W_{50}. In our case W_{50} = 0.110 kg. The diameter $D_{n50} = (W_{50}/\rho_s)^{1/3}$. or in our case D_{n50} = 0,033 m. The core material had W_{C50} = 0.0059 kg.

Wave measurements.

The wave measurements were carried out with wave gauges of the conductive type. Four wave gauges were used and positioned as shown in Figure 1. Three of the gauges were placed in a group some distance in front of the berm breakwater model and one gauge was placed just in front of the breakwater model. The three gauges were placed according to recommendations from Mansard and Funke (1980) with respect to analysis of incoming and reflected waves. The distance from the breakwater of these three gauges followed the recommendations from Goda (1985).

The measurements showed little variation of the standard deviation of the surface elevation between the three gauges. Hence the height of the incoming wave was taken as the mean of the waves measured at the three gauges. Since reflection was not a major issue in this study, the reflection coefficients were not obtained. Lissev (1993) analysed the incoming and reflected waves for an almost identical test set-up as we have used.

It was finally decided to carry out force measurement tests with two nominal peak wave periods: T_p = 2.0 and 2.4 s.

Wave force measurements on single armor unit.

The different armor stones on a berm breakwater have different sizes and shapes. They are embedded in each other in such a way that they will be exposed to the flow in a somewhat arbitrary way. The wave forces induced on a specific stone may for a certain wave condition thus vary with the sheltering effect it is subjected to from the neighbouring stones. To explore the forces on single stones will therefore require tests with several stones placed in different orientation and in different positions with respect to other stones. Since measurements of forces on sharp edge stones and associated water particle velocities had not been carried out before, Tørum (1992, 1994) carried out measurements for a single stone placed at one position and in one orientation on a berm breakwater to gain more insight into the mechanism of regular wave forces on an armor unit on a breakwater.

In the present study these wave force measurements were continued. We decided to carry out tests with irregular waves on an armor stone placed at different locations along the breakwater slope and with the stone in an embedded and elevated position at each location. The orientation of the stone was the same in each location.

The force measurements were made with a force transducer placed in a cylindrical box as shown in Figure 3. This box was then placed in the breakwater as shown in Figure 4 after the berm had been reshaped by waves to a stable profile. The box was originally made perforated with the intention to let water flow through it. However, it was finally decided to cover the holes with a plastic sheet in order to avoid any possible forces on the transducer from flowing water within the box.

To exclude any contact between the force measurement stone and neighbouring stones, a stiff chicken wire mesh was placed around the stone used for the force measurements.

There is also a question whether the instrumentation box had some influence on the flow velocities in the berm. The computer program ODIFLOCS ,van Gent (1992), was used to make some calculations of the flow velocities within the berm. Based on these calculations it was deemed that the influence from the force transducer box on the measured wave forces is not significant, Tørum (1994).

The force transducer is designed and built by MARINTEK A/S, SINTEF Group. The force transducer is based on measuring the strains in shear when the transducer is subjected to a force. The force transducer, shown in Figure 3, is a two-component force transducer. It was orientated such that the wave forces parallel and normal to the breakwater slope was measured. Prior to mounting the force transducer into the breakwater it was calibrated with a known force up to 1 N.

The force measuring stone had a mass of 0.152 kg and a specific density of 3.050 kg/m^3. The volume of the stone was 0.000049 m^3 (49 cm^3). The projected area in the direction parallel to the breakwater slope was 0.0018 m^2 (18 cm^2) while the projected area normal to the breakwater slope was 0.00185 m^2 (18.5 cm^2).

In this present study we did not measure water particle velocities similar to what Tørum (1992,1994) did. This was partly because in most positions where we measured wave forces the waves would break and airbubbles in the water would create problems for water particle velocity measurements with a laser Doppler velocity meter, which was used in the previous study. Instead we concentrated on doing the force measurements for irregular waves and treating the wave forces statistically.

The location of the force measurement points is shown in Figure 5.

The co-ordinates for the measurement points are given in Table 1.

In all points, except Point A, the measurement stone was placed in an embedded position and in an elevated position. In the embedded position the stone was embedded among the other stones and the top of the stone was more or less in the same position as the top of the neighbouring stones. In the elevated position the underside of the stone was more or less at the

top of the neighbouring stones. The elevated position thus resembled the position a rolling stone would have at a certain time point. In point A the stone was only placed in an embedded position because there were problems to place the stone in an elevated position on the rather steep slope at point A.

Table 1 Co-ordinates for the measurement points, Figure 5.

Point	Horizontal axis,	Vertical axis, m
A	-0.1275	0.085
B	0	0
C	0.22	-0.055
D	0.65	-0.17

Point D is the same as used by Tørum (1992, 1994).

The natural frequency of the force transducer was such that there was some dynamic effects on the measured force. This will be dealt with in more detail under the chapter on data analysis.

Tests and test procedures.

After the wave calibration runs had been completed, the breakwater model was rebuilt. A series of large waves, up to H_s~0.3 m, was then run to reshape the breakwater model.

The wave force transducer was then mounted into the berm.

To limit the test program it was decided to run tests with two different wave periods and two different wave heights for each wave period. The test program is shown in Table 2. The following notation applies:

H_s = significant waveheight = $4\sqrt{m_0}$
m_0 = area under the wave spectrum
T_p = peak period
T_z = mean zero up-crossing period ≈ $T_p/1.4$.
$\Delta = (\rho_s/\rho_w) - 1$
ρ_s = specific mass of the stone = 3050 kg/m^3
ρ_w = specific mass of the water = 1000 kg/m^3
$D_{n50} = (W_{50}/\rho_s)^{0.333}$ = 0.033 m.
W = mass of individual stones
W_{50} = 50 % of the stones have a larger (or smaller) mass than W_{50} = 0.110 kg.
g = acceleration of gravity = 9.81 m/s^2

A value of Ho =1.9 represents a wave condition for which there is almost no motion of the stones on the berm, while for a value of Ho = 2.65 there is some movement of the stones.

Table 2. Test program.

T_p , s	H_s , m	$Ho=H_s/\Delta D_{n50}$	$s=2\pi H_s/gT_z^2$
2.0	0.13	1.90	0.041
	0.18	2.65	0.057
2.4	0.13	1.90	0.028
	0.18	2.65	0.039

The tests started with the force measuring stone in Position D. The run time for each test series was then 500 s (or 300 -350 waves). The sampling interval was 0.05 s. The time series was then fairly smooth and there were no signs of impulsive forces on the stone.

The wave force measuring stone was the moved to position B. It appeared then to be impulsive type forces on the stone with apparently high, short duration forces. The sampling time was then changed to 0.002 s. Due to capacity limitation of the data storage system the run time for each test series had then to be reduced to 180 s (or 105 - 125 waves).

It appeared that the significant wave height calculated from the first 105 waves were approximately 10% larger than the significant wave height calculated from the first 300 waves, including the 105 waves. A visual inspection of the time series of the waves showed clearly that the larger waves appeared among the first 105 waves.

Time did not allow to go back and repeat the tests in Point D with a sampling interval of 0.005 s. Hence there might be some differences in the analysed forces for Point D and the other points from the fact that a somewhat different test and analysis procedure were used for Point D.

Analysis and results.

We will in this chapter summarise the analysis and the main results of the study. The thesis of Ketil Westeren (1995) and the report of Tørum (1997) includes more time series, graphs etc. than will be presented in this paper.

General on the measured forces.

The zero force was taken as the force read when there were still water conditions in the wave flume. This means that for the measurements in Points C and D the buoyancy force is automatically deducted in the measurements. This applies also for the measurements in Point C, embedded stone case. For the measurement Point A and measurement Point B, elevated stone case, the buoyancy force is included in the measured forces. The buoyancy force for the force measuring stone in still water is 0.49 N. The buoyancy force for a stone on a slope subjected to waves have direction normal to the instantaneous slope of the water surface (under the assumption of quasi hydrostatic conditions). It is thus quite laborious to sort out the buoyancy force for a stone that is partly in water and partly out of water for all the waves we have run.

In all our analysis we have used the measured forces and not included any considerations on buoyancy being or not being automatically accounted for. In the discussions we will revert to this question.

Figures 6 and 7 show characteristic forms of the wave forces for the different measurement points.

It was mentioned that there might be a dynamic amplification on the response of the force transducer related to the stiffness of the force transducer. This applies especially to the forces in Points A and B. The forces in these points have to some extent character of impulse forces. Figure 8 shows part of a time series for the horizontal force in Point B. This force or rather the force transducer response time trace has the appearance of the response of a system with a natural period of oscillations close to 0.1 s.

It is a well known fact that breaking waves may give slamming forces, e.g. Kyte and Tørum (1996).

A stone could be approximated by a sphere in the respect of slamming forces. We have not at hand any investigation on slamming forces on spheres. We will therefore consider the slamming forces on a cylinder.

von Karman (1929) derived the following expression for the slamming force on a cylinder of length L and diameter D:

$$F_s = \rho_w C_S (1 - \frac{t}{\tau}) DL v_s^{\ 2}$$

where v_s = relative velocity between water and cylinder
C_S = coefficient. Theoretically derived by von Karman: $C_S = \pi$.
t = time
$\tau \sim \frac{D}{2v_s}$, duration time for the slamming force.

An approximate duration time of a slamming force on the force measuring stone in position A is arrived at through the following reasoning:

The wave force measuring stone we used had an equivalent diameter $D_n = (W/\rho_s)^{0.333} \sim 0.037$ m. van Gent's (1995) velocity calculations is for a model berm breakwater of almost the same size as the berm breakwater model and waves used in the present study. From van Gent's calculations we deem the maximum velocity at Point A to be approximately 1.00 m/s. An approximate duration time of a slamming force will then be $\tau \approx 0.02$ s.

The wave force measuring stone was plucked while located in Point A. The force measuring stone was during the pluck tests located above water. Figure 9 shows the time trace for the response of the force transducer to the plucking. The natural period of oscillation is approximately 0.1 s. The pluck test also indicate that the force measuring system is heavily damped, possibly partly because the transducer is submerged in water.

We do not know the exact force - time history for the impulsive force from the waves running up the slope, to some extent as plunging breakers.

Western (1995) used to him readily available response results for a rectangular pulse load to investigate the possible dynamic influence on the response of the force transducer. Tørum (1997) have elaborated further on this item and the main results are included here. The dynamic response of a single-degree-of-freedom system on a rectangular pulse with duration t_o and natural period of oscillation of $T_n = 0.1$ s is shown in Figure 10 for two damping ratios ξ = ksi = 0.05 and 0.5. $\xi = c/c_{cr}$, c_{cr} = critical damping, c = actual damping. Figure 11 shows the theoretical response of the same system for an impulse load ("pluck").

The pluck test results shown in Figure 11 compared with the theoretical pluck response shown in Figure 9 indicates that the damping in the force measuring system is high, may be as high as $\xi = 0.5$.

If the duration of the impulse is 0.1 s, calculations indicate then that the amplification factor is 1.1. However, the theoretical calculations indicate that the duration of the impulse load may be shorter. The dynamic amplification factor will then be lower than 1.0, may be as low as 0.7.

The forces that we "measure" will thus inherently be uncertain, especially in the locations Point A and Point B, where the forces to some extent are of impulsive character.

A closer inspection of the time series of the forces show that there is a phase difference between the parallel and normal forces, Westeren (1995), Tørum (1997). This was also observed by Tørum (1992, 1994).

Analysis of the measurement results.

If we apply the von Karman (1929) expression for the impact force (see previous chapter) and assume L = D = 0.037 m, $v_s = 1.0$ m, $C_S = \pi$ and $\rho_w = 1000$ kg we arrive at a maximum force of $F_{max} = 4.5$ N, while the maximum measured force on the measurement stone is approximately 4 N. This does not give any proof to the formulae, but indicates that the forces are in the ballpark "correct".

There could be different ways of analysing the data. We have chosen a statistical analysis of the forces, basically because we are dealing with irregular waves.

We have previously discussed the uncertainty of the force measurements, especially in Point A and Point B, where the forces to some extent were of impulsive character. In the analysis it has not been possible to make any corrections to the data. Hence we have analysed the data as they are and will revert to the uncertainties in the chapter "Discussions".

We have fitted a Weibull distribution function to the force data. The fitting has been according to the method of moments.

The Weibull distribution function is given by:

$$P(F_{peak}) = 1 - \exp(-\frac{F_{peak} - F_0}{F_c})^{\gamma}$$

where F_{peak} = force peak value
F_o = location factor
F_c = scale factor
γ = shape factor

The analysis program STARTIMES, Hoen and Brathaug (1987), was used to analysed the data. To avoid all the small peaks in the time trace a lower limit of 0.1 N was set for a peak value. Also the time difference for two consecutive peak values was set to a fixed value , slightly less than the peak period.

Figure 12 shows the fitted Weibull distribution to the upward directed parallel force data from measurement Point D for one wave condition. Similar diagrams were found for the downward forces and the normal forces for the different measurement positions and wave conditions.

The Weibull fit is reasonable as was also the case for most of the other wave conditions and measurement points.

The obtained shape factors for the embedded stone case, parallel force, is shown in Figure 13. The "negative" values of the shape factor signifies the shape factors (which always are positive) for the downward parallel forces. The shape factors for the other forces and test conditions are found in Western (1995) and Tørum (1996).

The shape factor varies between 1 and 2. However, there is no uniformity of the variation. It can therefore not be concluded that there is a "universal" Weibull law on the force distribution.

In order to extract possible significant differences on the forces for the different conditions and to be able to draw some more general conclusions we picked out what we designated the 90% and the 99% forces for each test series. The 90% and 99% force was defined as the force with a 90% and a 99% probability respectively of not being exceeded. These forces were taken from the fitted theoretical Weibull distributions. As an example the 90% and 99% forces taken from Figure 12 is 0.42N and 0.65N respectively.

Figures 14 and 15 show the 90% parallel and normal forces at the different measurement points for different wave conditions for the embedded stone case. Figures 16 and 17 shows the same results for the elevated stone case. Similar results for 99% forces are shown in Westeren (1995) and Tørum (1996). The results show that the forces are highest above the still water line, measurement Point A. The results also show, as expected, that the forces are higher for the embedded stone case than for the elevated stone case.

Discussions.

Prior to formulating the test program we had some reasoning that the highest forces might be occurring at the flattest slope and at the still water line because it would take the highest forces to move the stones on this part of the breakwater. Water particle calculation as calculated for example by van Gent (1995) show that the highest velocities apparently occurred at or slightly below the still water line, indicating that the forces might be highest in this region.

We measured the highest forces above the still water line. Although there are some uncertainties on the measured forces, it seems to be safe to say that the forces are highest in the region above the still water line. These forces have the character of slamming forces and the question may be raised that these forces have so short duration that they will not be able to move the stones. We know, however, that slamming forces on for example vertical breakwaters are able to move the rather heavy breakwater. Hence there is no doubt that slamming or quasi slamming forces on an armour unit on a berm breakwater will be able to move the unit. Hence a mechanism for moving the stones may be that they are gradually "knocked" loose by the slamming forces and than moved further up or down the slope.

It is interesting to note that, generally speaking, the parallel forces are highest for the longest wave peak periods provided the significant wave heights are the same. This means that the waves with the lowest steepness give the highest forces. It is interesting to note that the waves with the lowest steepness, provided the same significant wave height, have the largest reshaping effect on the berm of a berm breakwater, e.g. Archetti et al (1995).

The present tests were carried out with a depth of water in front of the breakwater such that the waves did not break until they broke on the breakwater. Tørum (1997) dealt with three dimensional (3D) tests on a berm breakwater head in shallow water with wave conditions where the largest waves broke before they came to the breakwater and where the ratio H_{max}/H_s is smaller than expected in deep water. For the shallow water tests Tørum found that the recession of the berm is smaller than for deep water tests, Alikhani et al (1996). There might be different reasons for this, which is discussed by Tørum (1997). But one of the reasons is probably that the maximum wave forces on single armor units are smaller under breaking wave conditions in shallow water than without breaking in deeper water. Hence the ability to reshape the berm is less for shallow water breaking waves than for deep water non-breaking waves, because the maximum waves in shallow water are smaller than in deep water, although the significant wave heights are the same in the shallow and deep water case.

The normal forces are generally speaking smaller than the parallel forces. For the "embedded stone" case the normal forces are of the same magnitude in Points B, C and D, while they are larger in Point A (above the still water line). When we consider that the normal forces for the "embedded stone" case in Point A also include a buoyancy component we see that the downward vertical wave force is considerable, which again probably is caused by a slamming force effect. This vertical downward force is a stabilising force on the stone. However it might induce some "shaking" of the stone, which, together with the induced parallel force induce a total shaking of the stone as part of the mechanism for "knocking" loose the stones.

The stability of a single armor unit depends on the forces on the unit. The concept we have for the dislocation and motion of the stone is that it either rolls, slides or jumps along the slope. If

we consider the rolling concept, Figure 18 , the following relation has to be fulfilled in order for the stone to roll:

$F_N r_N + F_P r_P \geq W r_W$

where W = submerged weight of the stone
F_N = normal force
F_P = parallel force
r_W, r_N, r_P = the arms for the respective forces.

Although the force arms, r, are unknown and will vary from stone to stone, we will, for an order of magnitude calculation, as a reasonable assumption set $r_W = r_N \cos\alpha$, $r_N = 0.5\ D_n$ and $r_P = 0.25\ D_n$ and α = slope angle.

The submerged weight of the stone is set equal to:

$Q = g(\rho_s - \rho_w)\ V_s$ when buoyancy is taken into account, Point C and D and partly Point B during the present force measurement project.

and $W = g\rho_s V_s$ when buoyancy is not taken into account, point A and partly point B during the present force measurement project.

where g = acceleration of gravity = 9.81 m/s^2
ρ_s = specific mass of the stone = 3050 kg/m^3
ρ_w = specific mass of the water = 1000 kg/m^3
V_s = volume of the stone = 0.000049 m^3 for the force measuring stone.

With these assumption we obtain:

$F_N + 0.5\ F_P \geq 0.98 \cos\alpha$ (N) when the buoyancy is taken into account

and $F_N + 0.5\ F_P \geq 1.46 \cos\alpha$ (N) when the buoyancy is not taken into account.

The slope angles in the different measurement points are approximately as shown in Table 3.

Table 3. Slope angle at different force measurement points.

	Slope angle, α, degrees	cos α
Point A	33.6	0.83
Point B	25.0	0.90
Point C	12.0	0.98
Point D	10.0	0.98

Inspections of the different force-time recordings show that in no case is the upward normal force exceeding 0.98 N in Points B, C and D. In Point A the upward normal force do not

exceed 1.46N. Hence the normal force alone will not be able to dislocate the force measuring stone if it was free to move.

In Points A and B the combination of normal and parallel forces would be able to move the stone both in the embedded and the elevated position.

In Point C the combination of parallel forces and normal forces would just be able to move the stone from its embedded location, while it easily would be movd in an elevated position.

In Position D the stone would not move in its embedded position, while it would move in its elevated position.

Conclusions.

The measured wave forces on an individual armor stone on a berm breakwater have given new insight in the complex mechanism of the interaction between the waves and the stones. The measurements show that the highest forces occur above the still water line. The forces in this region have to some extent the character of "slamming" forces with a short duration. However, it is believed that these forces are able to gradually "shake" the stones and "knock" them loose into an "elevated" position from which they are transported down the slope.

Acknowledgement.

This project was carried out under the European Communities Research Program "Marine Science and Technology", EC MAST II. More specifically the project was carried out under the project EU MAST II Berm Breakwater Structures - Contract MAS2-CT94-0087. The project was also funded by the Norwegian Coast Directorate (50%). We appreciate very much the financial support from EC and Norwegian Coast Directorate.

The writers are also grateful to the other participants of the project for discussions and comments during workshops.

References.

Alikhani, A., Tomasicchio, R. and Juhl, J. (1996) Berm breakwater trunk exposed to oblique waves. Proc. 25th International Conference on Coastal Engineering, Orlando, Florida, 2 - 6 September 1996.

Andersen, O.H., van Gent, M., van der Meer, J.W., Burcharth, H.F. and den Adel, H. (1993): Non-steady oscillatory flow in coarse granular materials. EU-MAST I Coastal Structures, Project 1.

Andersen, O.H. (1993): Flow in porous media with special reference to breakwater structures. PhD thesis, Hydraulic and Coastal Engineering Laboratory, Aalborg University, Aalborg, Denmark.

Archetti, R. and Lamberti, A. (1995). Reshaping breakwater: Profile parametrisation. MAST II Berm Breakwater Structures. 3rd workshop, Stavanger 10 May 1996.

Brandtzæg, A. and Tørum, A. (1966) A simple mathematical model of wave motion on a rubble mound breakwater front. Proceedings 10th International Conference on Coastal Engineering, Tokyo, Japan, 1966.

Brandtzæg, A., Tørum, A. and Østby, O.R. (1968): Velocities in downrush on rubble mound breakwaters. Proceedings 11th International Conference on Coastal Engineering, London. Great Britain. ASCE pp 815 - 832.

Breteler, M.K. and van der Meer, J.W. (1990): Measurement and computation of wave induced velocities on a smooth slope. Proceedings 22nd International Conference on Coastal Engineering, ASCE, New York, NY pp 191-204.

Cornett, A. and Mansard, E. (1994): Wave stress on rubble mound armour. Proc. 24th International Conference on Coastal Engineering, Kobe, Japan.

Fisher, M., Juhl, J. and Rasmussen, E.B. (1992): Numerical modelling of waves and currents with regard to coastal structures. Proceedings 23rd International Conference on Coastal Engineering, Venice, Italy, october 1992, pp 170-183.

Forchheimer, P. (1901): Wasserbevegung durch Boden. Z. Ver. Deutsch Ing. Vol 45 pp 1782 - 1788.

Goda, Y. (1985): Random seas and design of maritime structures. University of Tokyo Press.

Hedar, P.A. (1960): Stability of rock-fill breakwaters. Dr. thesis no. 26, Chalmers Technical University, Gothenburg, Sweden.

Hoen, Chr. and Brathaug, H.P. (1987): STARTIMES. SINTEF Report STF71 A87047. SINTEF, 7035 Trondheim, Norway.

Hudson, R. (1958): Design of Quarry Stone Cover Layers for Rubble Mound Breakwaters. Waterways Experiment Station, Research Report No 2-2, 1958.

Iwata, K., Miyazaki, V. and Mitzuani, N. (1985): Experimental study of the wave force acting on rubble mound slope. Natural Disaster Sci., 7(2), 29-41.

Jensen, O.J. and Juhl, J. (1988): Results of model tests on 2-D breakwater structures. Proceedings of the Conference "Breakwaters '88" organized by the Instituion on Civil Engineers and held in Eastbourne on 4-6 May 1988, pp 13-25.

Juhl, J. and Jenssen, O.J. (1990): Wave forces on breakwater armor units. Proceedings of the 22nd International Conference on Coastal Engineering, Delft, The Netherlands, 2-6 July 1990. ASCE pp 1538-1551.

Kobayashi, n:, Otta, A.K. and Ray, I. (1986): Numerical simulation of wave run-up and armour stability. OTC Paper 5088, 18th Offshore Technology Conference. Vol 1, Houston, Texas, pp 51-56.

Kobayashi, N., Otta, A.K. and Ray, I. (1987): Wave reflection and run-up on rough slopes. Journal of Waterway, Port, Coastal and Ocean Engineering, Vol 113, No 3, May 1987, pp 282-298.

Kobayashi, N. and Wurjanto, A. (1989): Numerical model for design of impermeable coastal structures. Center for Applied Coastal Research, Department of Civil Engineering, University of Delaware, Newark, Delaware, 19716, USA. Research Report No CE-89-75, June 1989.

Kyte, A. and Tørum, A. (1996): Wave forces on vertical cylinders upon shoals. Coastal Engineering, 27 (1996) 263 - 286.

Lissev, N. (1993) Influence of the core configuration on the stability of berm breakwaters Report R-6-93. Department of Structural Engineering, University of Trondheim, Norwegian Institute of Technology.

Lissev, N. and Tørum, A. (1996) Influence of the core configuration on the stability of berm breakwaters. Proceedings of the 25th International Conference on Coastal Engineering, Orlando, Florida, USA, 2 - 6 September 1996.

Losada, M.A., Medina, R. and Alejo, M. (1988): Wave forces on armor blocks. Proc. 21st International Conference on Coastal Engineering, Malaga, Spain, ASCE, pp 2479-2488.

Mansard, E.P.D. and Funke, E.R. (1980). The measurement of incident and reflected spectra using a least square method. Proceedings of the 17th International Conference on Coastal Engineering, Sidney, Australia, 1980.

Morison, J.R., Johnson, J.W. and O'Brien, M. (1953): Experimental studies on wave forces on piles. Proceedings of 4th Conference on Coastal Engineering. ASCE.

Rufin, T.M., Katsuhiko, K. and Iwata, K. (1994): Wave forces acting on armor unit of a submerged wide-crown breakwater. Proc. of the Fourth International Offshore and Polar Engineering Conference, Osaka, Japan, April 10-15 1994.

Sakakiyama, T. and Kajima, R. (1990): Scale effect of wave forces on armor units. Proceedings of the 22nd International Conference on Coastal Engineering, Delft, The Netherlands, 2-6 July 1990, pp 1716-1729.

Sandstrøm, Å. (1973): Wave forces on blocks of rubble mound breakwaters. Bulletin No 83. Dept. of Civil Engineering, Royal Institute of Technology, Stockholm, Sweden.

Sawaragi, T., Iwata, K. and Kobayashi, N. (1982). Conditions and probability of occurence of resonance on steep slopes of coastal structures. Coastal Engineering in Japan, vol. 25, 1982.

Sigurdson, G. (1962): Wave forces on breakwater cap-stones. Journal of the Waterways and Harbour Division, Proc. of the American Society of Civil Engineers, Vol. 88, WW 3 pp 27-60.

Tørum, A. (1992): Wave induced water particle velocities and forces on an armour unit on a berm breakwater. SINTEF Report STF A92 104, SINTEF 7034 Trondheim, Norway.

Tørum, A. (1994): Wave induced forces on armor unit on berm breakwaters. Journal of Waterway, Port, Coastal and Ocean Engineering, ASCE, Vol. 120, No 3, May/June 1994.

Tørum, A (1997): Berm breakwaters. Draft SINTEF Report. SINTEF, 7034 Trondheim, Norway.

Tørum, A. and van Gent, M. (1992): Water particle velocities on a berm breakwater. Proc. 23rd International Conference on Coastal Engineering, Venice, Italy, 4 - 9 October 1992.

van der Meer, J.W. (1988) Rock slopes and gravel beaches under wave attack. Delft Hydraulics. Publication number 396, 1988.

van der Meer, J. W., Petit, van den Bosch, P., Klopman, G. and R.D.Broekens (1992): Numerical simulation of wave motion on and in coastal structures, Proc. International Conference on Coastal Engineering, Venice, Italy, Vol. 2 pp 1772 - 1784.

van Gent, M. (1992): Numerical model for wave action on and in coastal structures. Communications on Hydraulic and Geotechnical Engineering, Report No 92-6. Faculty of Civil Engineering, Delft University of Technology, The Netherlands.

van Gent, M. (1993a): Berm breakwaters. Communications on Hydraulic and Geotechnical Engineering, Report No 93-11. Faculty of Civil Engineering, Delft University of Technology, The Netherlands.

van Gent, M. (1993b): Stationary and oscillatory flow through coarse porous media. Communications on Hydraulic and Geotechnical Engineering, Report No 93-9, Faculty of Civil Engineering, Delft University of Technology, The Netherlands.

van Gent, M., Peteit, H.A.H. and van der Bosch (1994): SKYLLA: Wave motions in and on coastal structures. Implementation and verification of flow on and in permeable structures. Report H1780. Delft Hydraulics, The Netherlands.

van Gent, M. (1995) Wave interaction with permeable coastal structures. PhD thesis, Delft University of Technology.

von Karman, T.H. (1929): The impact force on seaplane float during landing. NACA TN 321.

Westeren, K. (1995) Bølgekrefter på dekkstein på skuldermoloer. (Wave forces on armour units on berm breakwaters). MSc thesis Norwegian University of Science and Technology, Department of Structural Engineering. December 1995.

Notations.

c = damping
c_{cr} = critical damping
C_D = drag force coefficient
C_M = inertia force coefficient
C_L = lift force coefficient
C_s = slamming force coefficient
D = cylinder diameter
D_n = nominal stone diameter = $(W/\rho_s)^{1/3}$
D_{n50} = nominal 50% stone diameter = $(W50/\rho_s)^{1/3}$
Δ = $((\rho_s/\rho_w) - 1)$
F_p = parallel force
F_N = normal force
F_s = slamming force
F_{peak} = force peak value (Weibull)
F_0 = location factor (Weibull)
F_c = scale factor (Weibull)
g = acceleration of gravity
Ho = $H_s/\Delta D_{n50}$
H_s = significant wave height
L = cylinder length
m_0 = area under the wave spectrum
Q = submerged weight of stone
r_N, r_P,
r_w = arms for normal force, parallel force and weight force respectively.
T_p = peak period
T_z = mean zero-upcrossing wave period
t = time
v_s = "slamming" velocity
V_s = volume of stone
W = weight of berm stone (in air).
W_{50} = 50% of the berm stones are larger (or smaller) than W_{50}
W_{C50} = 50% of the core stones are larger (or smaller) than W_{C50}

γ = shape factor (Weibull)
ρ_s = specific mass of stones
ρ_w = specific mass of water
τ = duration time for slamming force
ξ = c/c_{cr}, damping ratio.

Figure captions.

Figure 1 Wave flume with test set-up.
Figure 2 Berm breakwater model cross section. (measurements in cm).
Figure 3 Force transducer: (a) Stone from above; (b) Facing flow; (c) From side.
Figure 4 Force transducer placed in the breakwater model (measurements in cm).
Figure 5 Location of the force measurement points.
Figure 6 Characteristic forms of the parallel and normal forces in Points B, C and D for the elevated stone case.
Figure 7 Characteristic form of the parallel and normal forces in Points A, B, C and D for the embedded stone case.
Figure 8 Expanded time series of a parallel force recorded in Point B (at still water line).
Figure 9 "Horizontal" response from a pluck test in Point A (above still water line).
Figure 10 Dynamic response of a single-degree-of-freedom system for $t_o = 0.02$ s and $T_n = 0.1$ s.
Figure 11 Relative "pluck" response of a single-degree-of-freedom system with $T_n = 0.1$ s.
Figure 12 Weibull distribution of the upward (positive) peak parallel forces in measurement Point D for $T_p = 2.0$ s and $H_s = 0.18$ m, embedded stone.
Figure 13 Shape factors, Weibull distribution, for parallel forces, embedded stone.
Figure 14 90% parallel forces for the embedded stone case.
Figure 15 90 % normal forces for the embedded stone case.
Figure 16 90 % parallel forces for the elevated stone case.
Figure 17 90 % normal forces for the elevated stone case.
Figure 18 The concept of rolling of an armor stone.

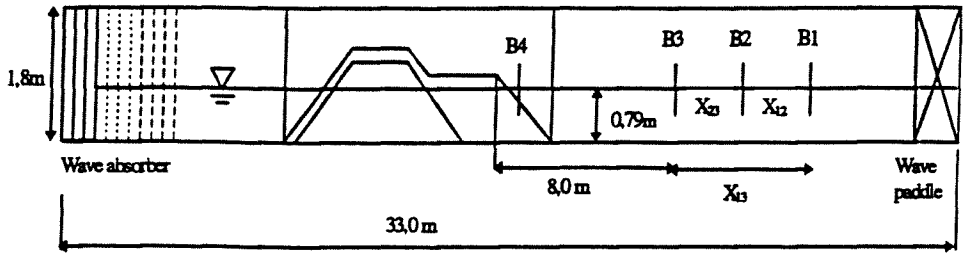
1,8m
B4
B3
B2
B1
0,79m
X_{23}
X_{12}
Wave absorber
8,0 m
X_{13}
Wave paddle
33,0 m

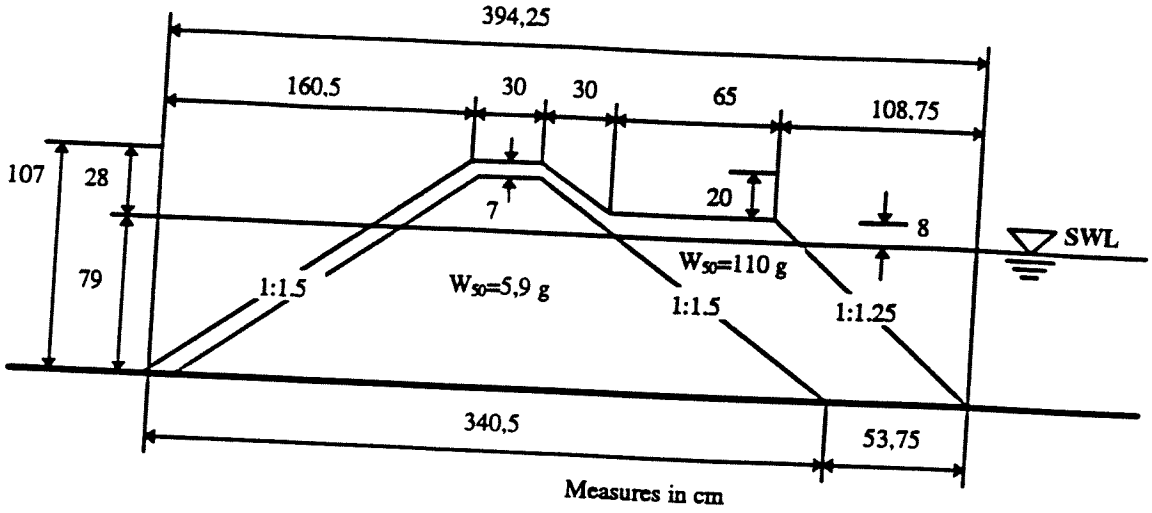
394,25
160,5
30
30
65
108,75
107
28
79
7
20
8
SWL
1:1.5
W_{50}=5,9 g
W_{50}=110 g
1:1.5
1:1.25
340,5
53,75
Measures in cm

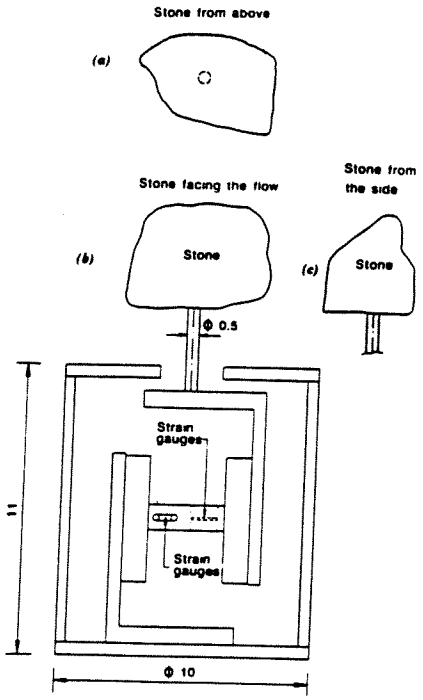
Stone from above
(a)
Stone facing the flow
Stone from the side
(b)
Stone
(c)
Stone
Φ 0.5
Strain gauges
Strain gauges
Φ 10

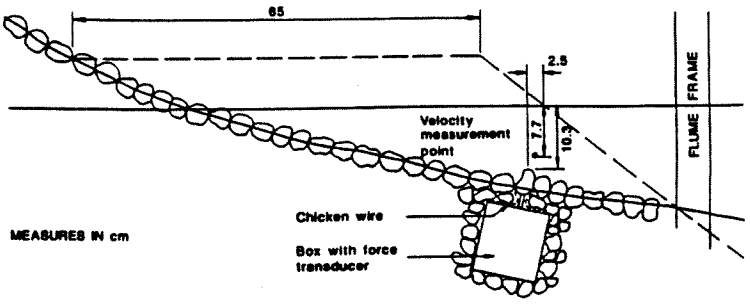
65
2.5
FRAME
FLUME
Velocity measurement point
7.7
10.3
Chicken wire
Box with force transducer
MEASURES IN cm

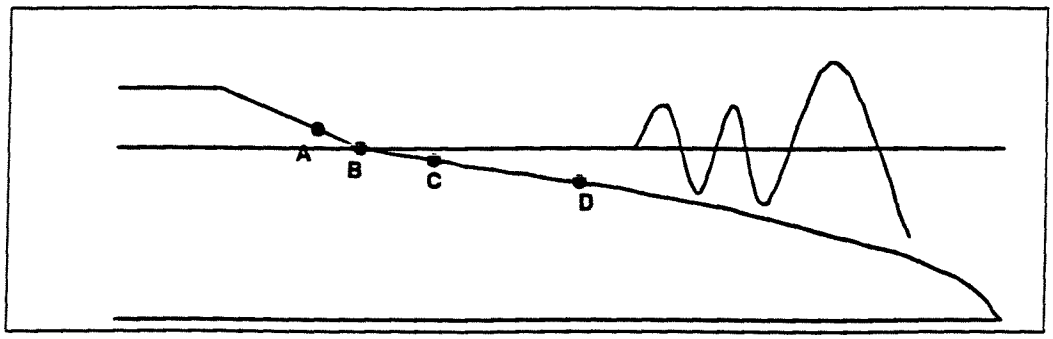
A
B
C
D

	T_p = 2.0 s. H_s = 0.18 m	T_p = 2.4 s. H_s = 0.18 m
Point B Parallel forces	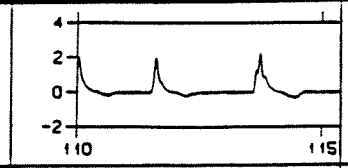	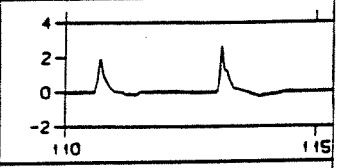
Point B Normal forces	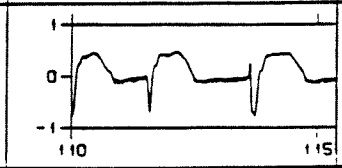	
Point C Parallel forces		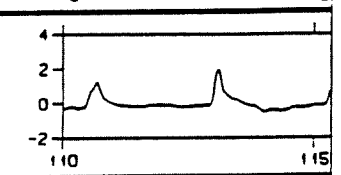
Point C Normal forces	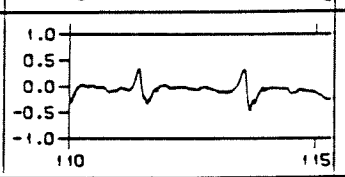	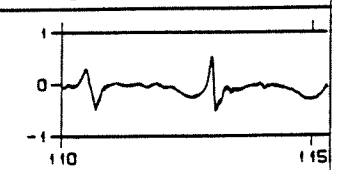
Point D Parallel forces		
Point D Normal forces	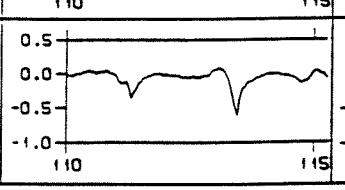	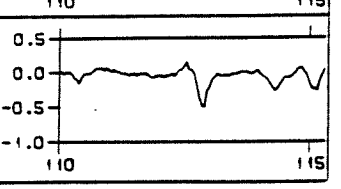

	T_p = 2,0 s, H_s = 0,18 m	T_p = 2,4 s, H_s = 0,18 m
Point A Parallel forces	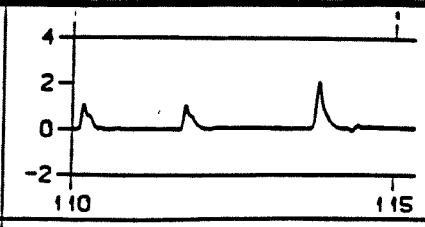	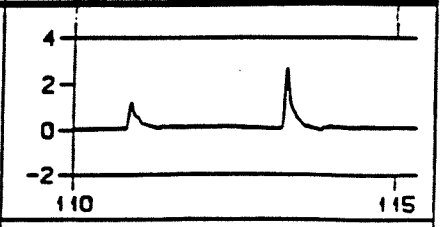
Point A Normal forces	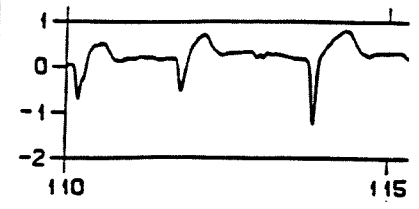	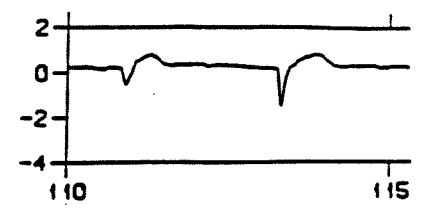
Point B Parallel forces	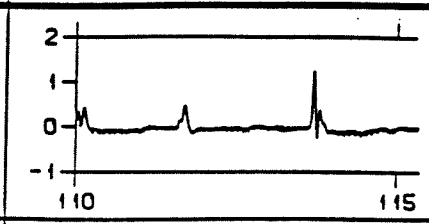	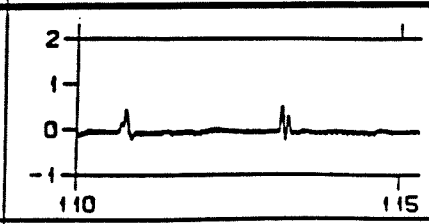
Point B Normal forces	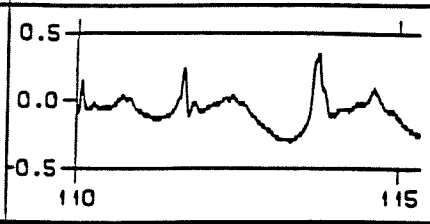	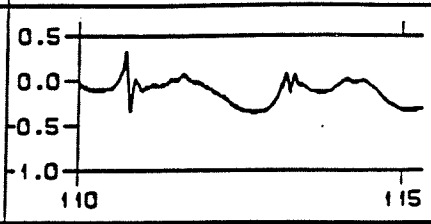
Point C Parallel forces	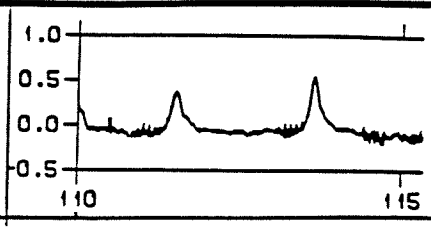	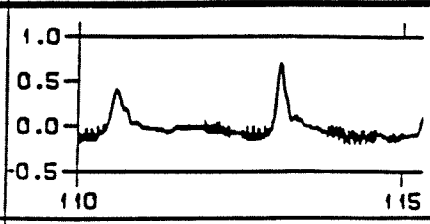
Point C Normal forces	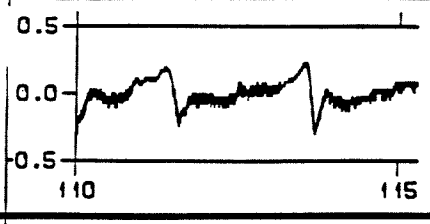	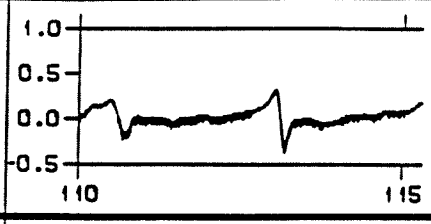
Point D Parallel forces	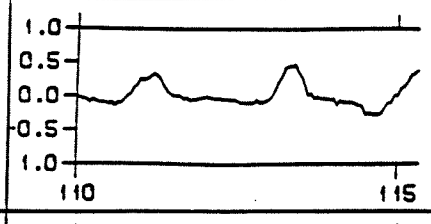	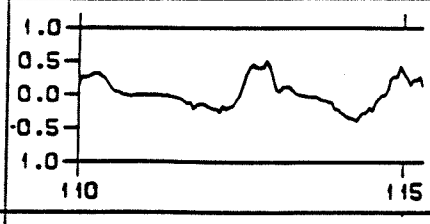
Point D Normal forces	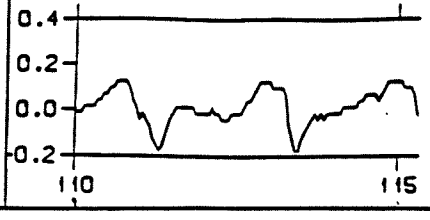	

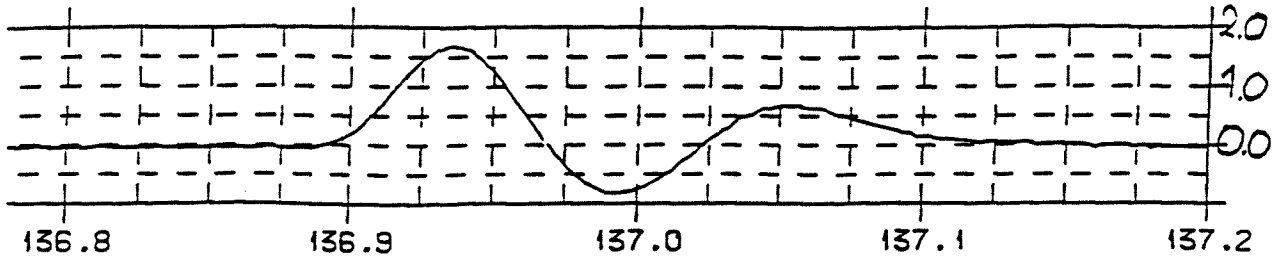
2.0
1.0
0.0
136.8
136.9
137.0
137.1
137.2

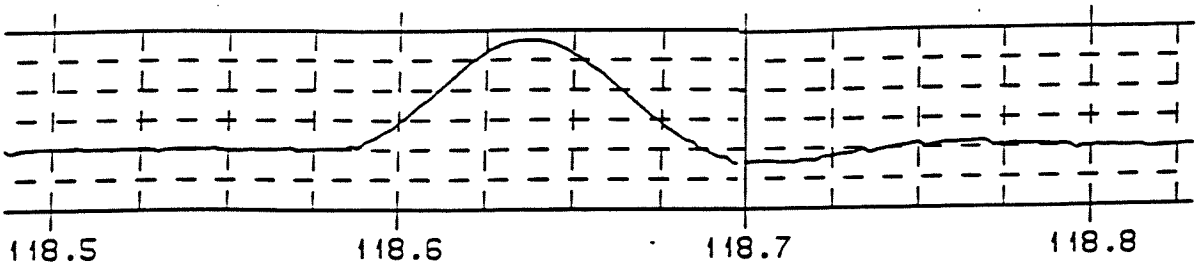
118.5
118.6
118.7
118.8

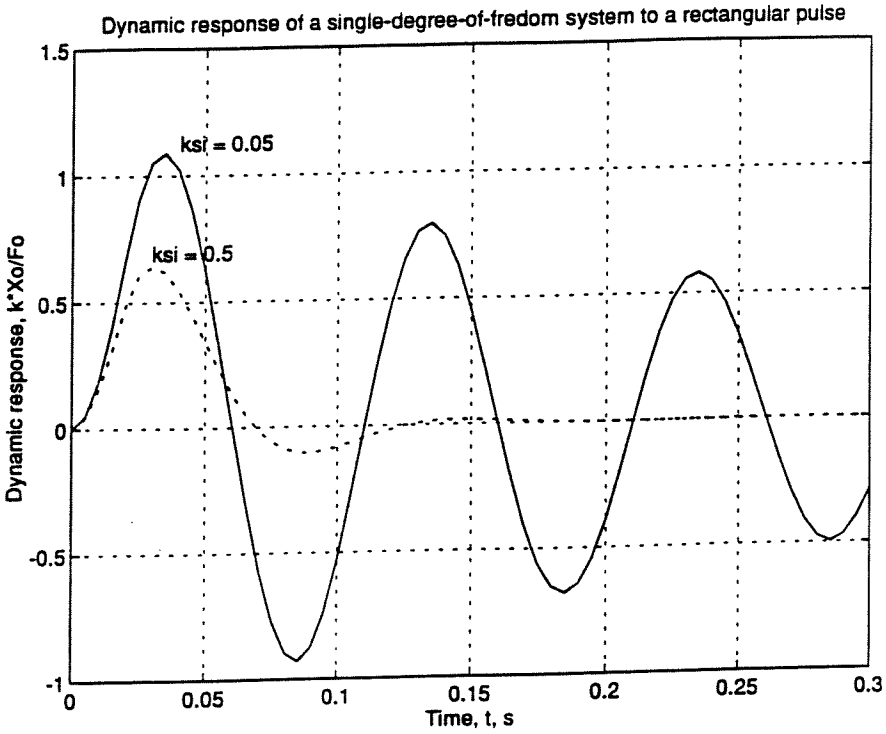
Dynamic response of a single-degree-of-fredom system to a rectangular pulse
ksi = 0.05
ksi = 0.5
Dynamic response, k*Xo/Fo
Time, t, s
1.5
1
0.5
0
-0.5
-1
0
0.05
0.1
0.15
0.2
0.25
0.3

Fig 1

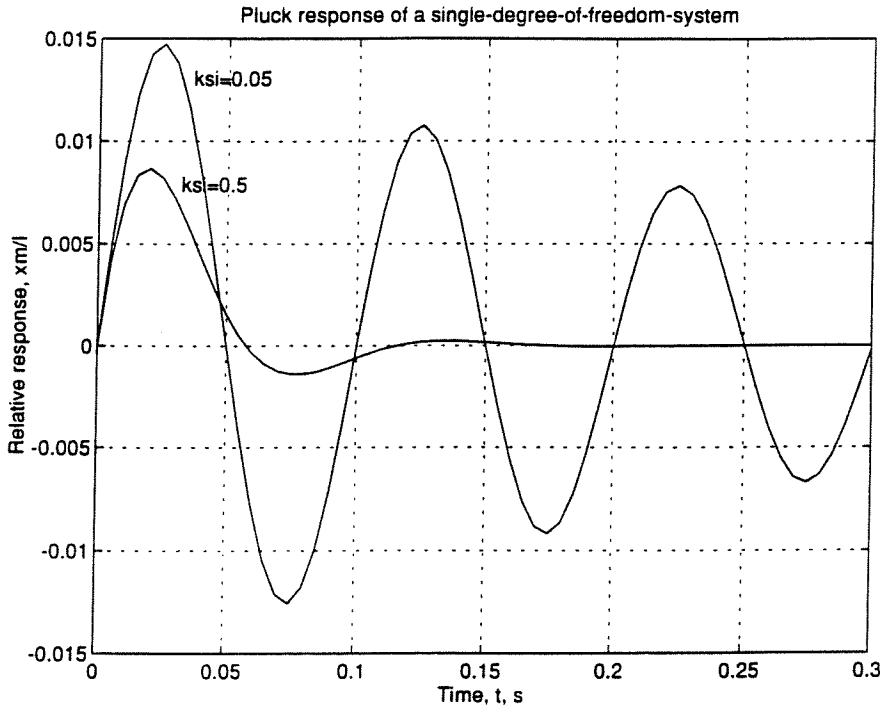
Pluck response of a single-degree-of-freedom-system
ksi=0.05
ksi=0.5
Relative response, xm/l
Time, t, s
0.015
0.01
0.005
0
-0.005
-0.01
-0.015
0
0.05
0.1
0.15
0.2
0.25
0.3

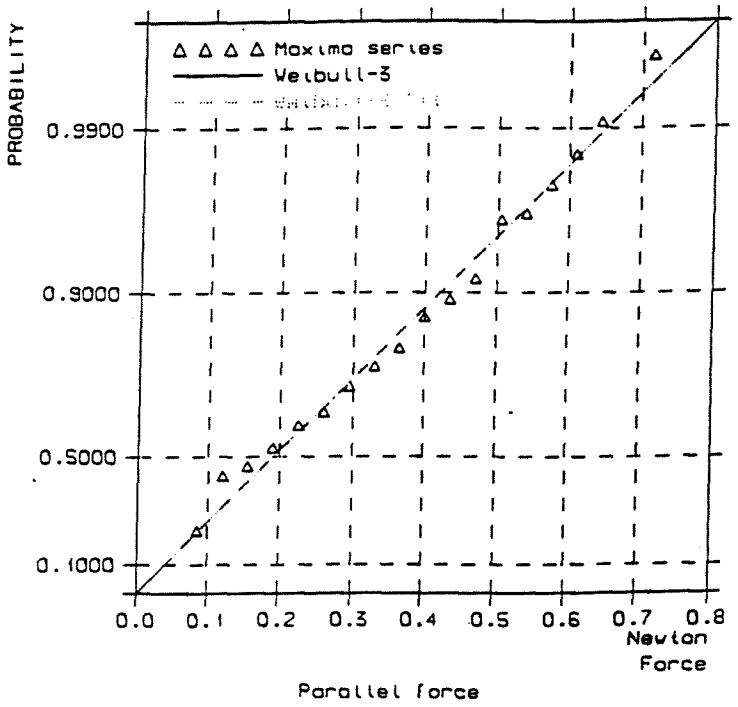
Maxima series
Weibull-3
PROBABILITY
0.9900
0.9000
0.5000
0.1000
0.0
0.1
0.2
0.3
0.4
0.5
0.6
0.7
0.8
Newton
Force
Parallel force

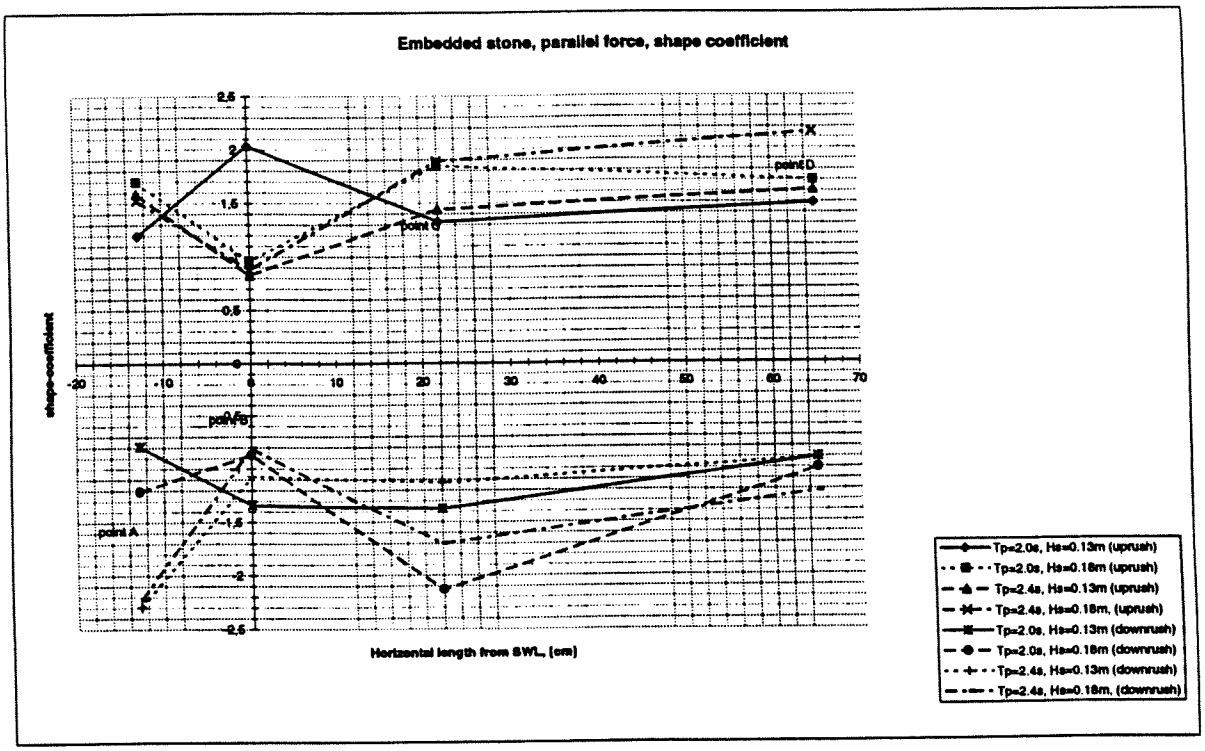
Embedded stone, parallel force, shape coefficient
shape-coefficient
Horizontal length from SWL, [cm]
point A
point B
point C
point D
Tp=2.0s, Hs=0.13m (uprush)
Tp=2.0s, Hs=0.18m (uprush)
Tp=2.4s, Hs=0.13m (uprush)
Tp=2.4s, Hs=0.18m, (uprush)
Tp=2.0s, Hs=0.13m (downrush)
Tp=2.0s, Hs=0.18m (downrush)
Tp=2.4s, Hs=0.13m (downrush)
Tp=2.4s, Hs=0.18m, (downrush)

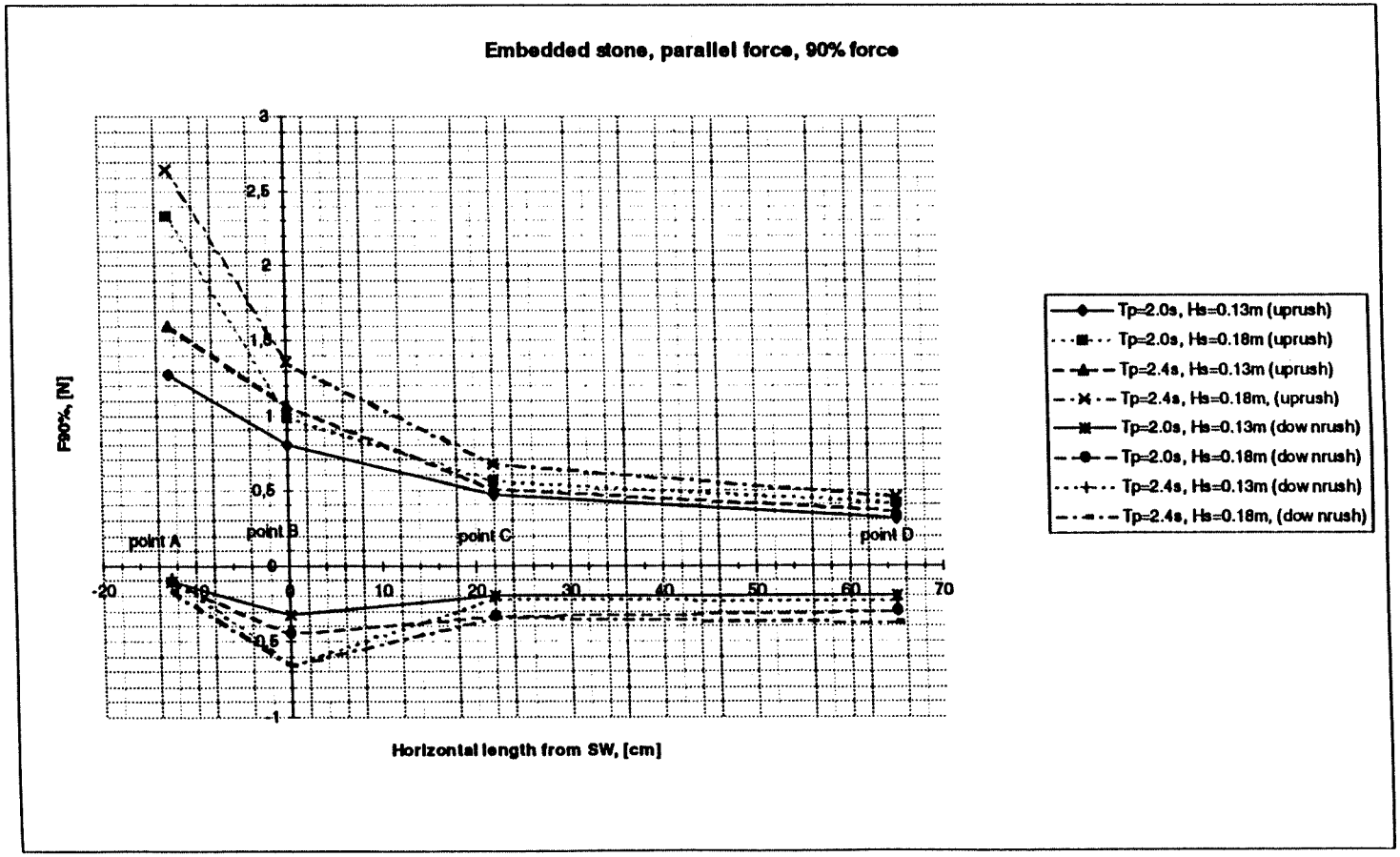
Embedded stone, parallel force, 90% force
F90%, [N]
3
2,5
2
1,5
1
0,5
0
-0,5
-1
-20
-10
0
10
20
30
40
50
60
70
point A
point B
point C
point D
Horizontal length from SW, [cm]
Tp=2.0s, Hs=0.13m (uprush)
Tp=2.0s, Hs=0.18m (uprush)
Tp=2.4s, Hs=0.13m (uprush)
Tp=2.4s, Hs=0.18m, (uprush)
Tp=2.0s, Hs=0.13m (down rush)
Tp=2.0s, Hs=0.18m (down rush)
Tp=2.4s, Hs=0.13m (down rush)
Tp=2.4s, Hs=0.18m, (down rush)

Fig 15

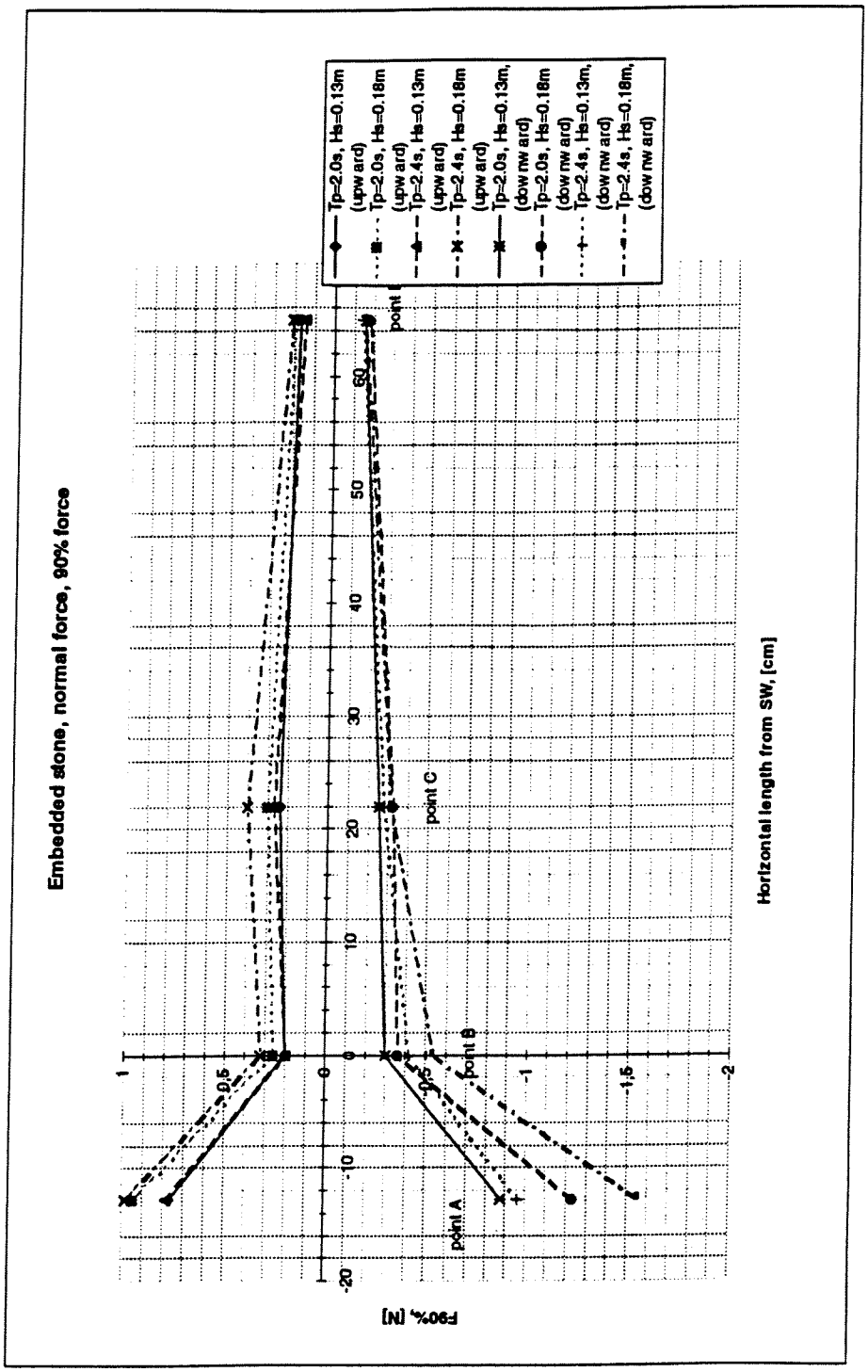
Embedded stone, normal force, 90% force
F90%, [N]
Horizontal length from SW, [cm]
point A
point B
point C
point
Tp=2.0s, Hs=0.13m (upw ard)
Tp=2.0s, Hs=0.18m (upw ard)
Tp=2.4s, Hs=0.13m (upw ard)
Tp=2.4s, Hs=0.18m (upw ard)
Tp=2.0s, Hs=0.13m, (dow nw ard)
Tp=2.0s, Hs=0.18m (dow nw ard)
Tp=2.4s, Hs=0.13m, (dow nw ard)
Tp=2.4s, Hs=0.18m, (dow nw ard)

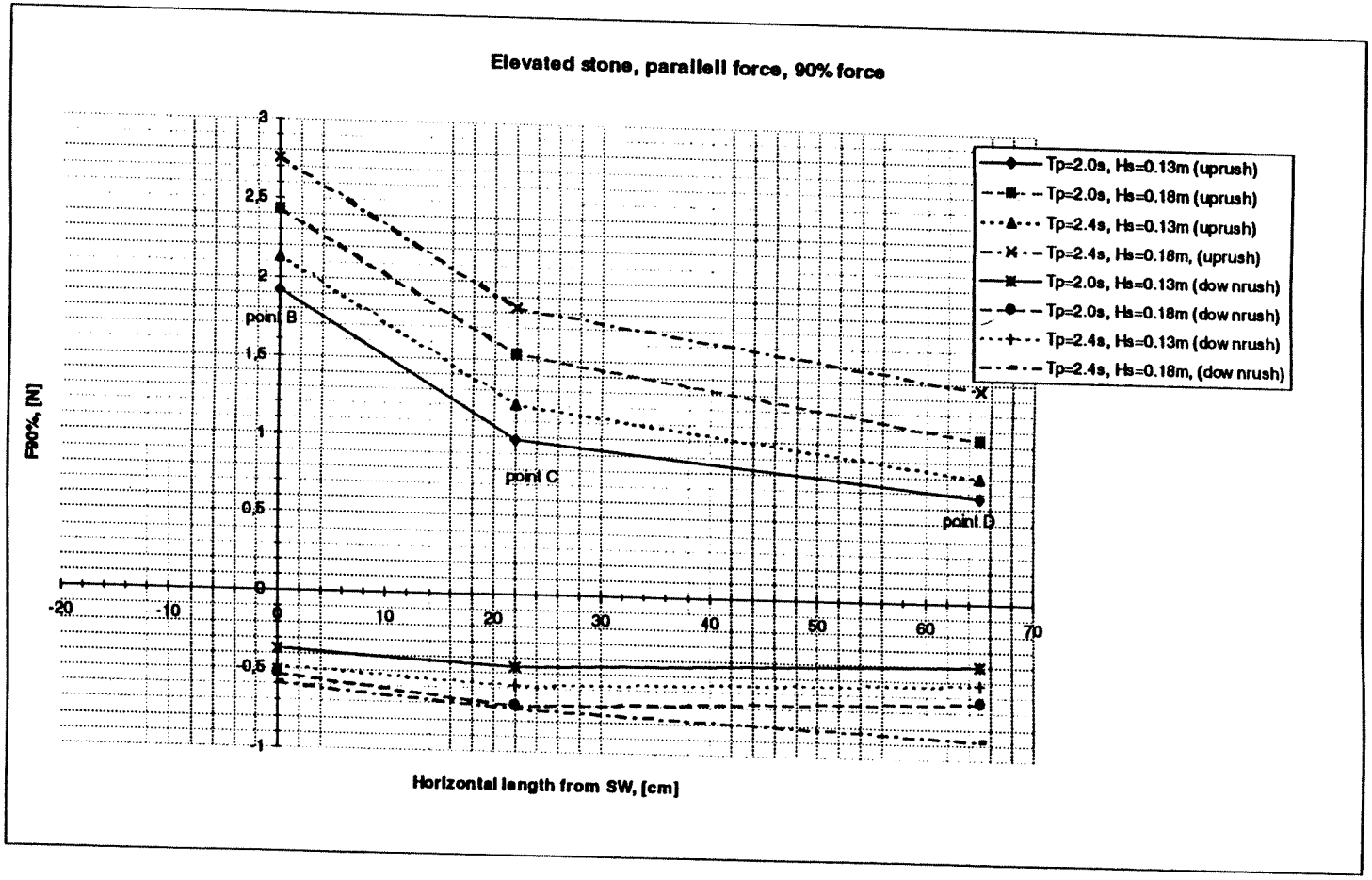
Elevated stone, parallell force, 90% force
F90%, [N]
Horizontal length from SW, [cm]
point B
point C
point D
Tp=2.0s, Hs=0.13m (uprush)
Tp=2.0s, Hs=0.18m (uprush)
Tp=2.4s, Hs=0.13m (uprush)
Tp=2.4s, Hs=0.18m, (uprush)
Tp=2.0s, Hs=0.13m (downrush)
Tp=2.0s, Hs=0.18m (downrush)
Tp=2.4s, Hs=0.13m (downrush)
Tp=2.4s, Hs=0.18m, (downrush)

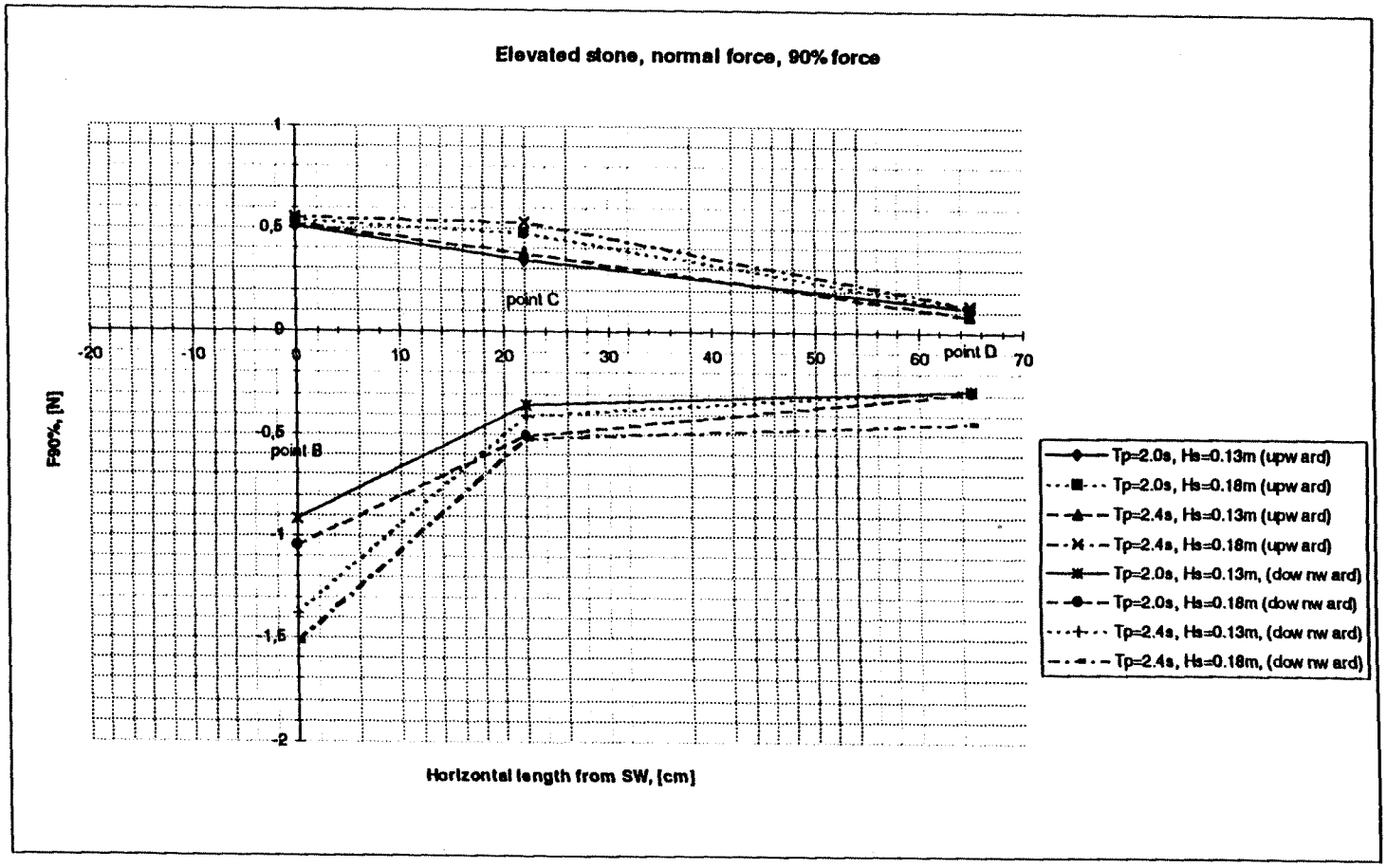
Elevated stone, normal force, 90% force
F90%, [N]
1
0,5
0
-0,5
-1
-1,5
-2
-20
-10
0
10
20
30
40
50
60
70
point C
point D
point B
Horizontal length from SW, [cm]
Tp=2.0s, Hs=0.13m (upward)
Tp=2.0s, Hs=0.18m (upward)
Tp=2.4s, Hs=0.13m (upward)
Tp=2.4s, Hs=0.18m (upward)
Tp=2.0s, Hs=0.13m, (downward)
Tp=2.0s, Hs=0.18m (downward)
Tp=2.4s, Hs=0.13m, (downward)
Tp=2.4s, Hs=0.18m, (downward)

Fig 18